1 **FRONT MATTER**

2 **Title**

3 Mid-Holocene Antarctic sea-ice increase driven by marine ice sheet retreat

4 **Authors**

5 Kate E. Ashley[1], Robert McKay[2], Johan Etourneau[3], Francisco J. Jimenez-Espejo[3,4], Alan Condron[5],

6 Anna Albot[2], Xavier Crosta[6], Christina Riesselman[7,8], Osamu Seki[9], Guillaume Massé[10], Nicholas R.

7 Golledge[2,11], Edward Gasson[12], Daniel P. Lowry[2], Nicholas E. Barrand[1], Katelyn Johnson[2], Nancy

8 Bertler[2], Carlota Escutia[3], Robert Dunbar[13] and James A. Bendle[1*].

9 **Affiliations**

10 [1]School of Geography, Earth and Environmental Sciences, University of Birmingham, Edgbaston,

11 Birmingham, B15 2TT, UK

12 [2]Antarctic Research Centre, Victoria University of Wellington, Wellington 6140, New Zealand

13 [3]Instituto Andaluz de Ciencias de la Tierra (CSIC), Avenida de las Palmeras 4, 18100 Armilla, Granada,

14 Spain

15 [4]Department of Biogeochemistry, Japan Agency for Marine-Earth Science and Technology

16 (JAMSTEC), Yokosuka 237-0061, Japan

17 [5]Department of Geology and Geophysics, Woods Hole Oceanographic Institution, Woods Hole, MA

18 02543, USA

19 [6]UMR-CNRS 5805 EPOC, Université de Bordeaux, 33615 Pessac, France

20 [7]Department of Geology, University of Otago, Dunedin 9016, New Zealand

21 [8]Department of Marine Science, University of Otago, Dunedin 9016, New Zealand

22 [9]Institite of Low Temperature Science, Hokkaido University, Sapporo, Hokkaido, Japan

23 [10]TAKUVIK, UMI 3376 UL/CNRS, Université Laval, 1045 avenue de la Médecine, Quebec City,

24 Quebec, Canada G1V 0A6

25 [11]GNS Science, Avalon, Lower Hutt 5011, New Zealand

26 [12]Department of Geography, University of Sheffield, Winter Street, Sheffield, S10 2TN, UK

27 [13]Department of Environmental Earth Systems Science, Stanford University, Stanford, A 94305-2115

28

29 [*]**Corresponding Author:** email: j.bendle@bham.ac.uk

30

1. ABSTRACT

Over recent decades Antarctic sea-ice extent has increased, alongside widespread ice shelf thinning and freshening of waters along the Antarctic margin. In contrast, Earth system models generally simulate a decrease in sea ice. Circulation of water masses beneath large cavity ice shelves is not included in current Earth System models and may be a driver of this phenomena. We examine a Holocene sediment core off East Antarctica that records the Neoglacial transition, the last major baseline shift of Antarctic sea-ice, and part of a late-Holocene global cooling trend. We provide a multi-proxy record of Holocene glacial meltwater input, sediment transport and sea-ice variability. Our record, supported by high-resolution ocean modelling, shows that a rapid Antarctic sea-ice increase during the mid-Holocene (~4.5 ka) occurred against a backdrop of increasing glacial meltwater input and gradual climate warming. We suggest that mid-Holocene ice shelf cavity expansion led to cooling of surface waters and sea-ice growth which slowed basal ice shelf melting. Incorporating this feedback mechanism into global climate models will be important for future projections of Antarctic changes.

44

2. INTRODUCTION

Ice shelves and sea ice are intrinsically linked and represent fundamental components of the global climate system, impacting ice-sheet dynamics, large-scale ocean circulation, and the Southern Ocean biosphere. Antarctic ice-shelves with large sub-shelf cavities (e.g. Ross, Filchner-Ronne) play a key role in regional sea-ice variations, by cooling and freshening surface ocean waters for hundreds of kilometres beyond the ice shelf edge (Hellmer, 2004; Hughes *et al.*, 2014). Antarctic sea ice has expanded over the past few decades, particularly in the western Ross Sea region (Turner *et al.*, 2016), alongside widespread thinning of ice shelves (Paolo *et al.*, 2015) and freshening along the Antarctic margin (Jacobs *et al.*, 2002; Aoki *et al.*, 2013). The drivers and feedbacks involved in these decadal trends are still poorly understood, hampered by the sparse and short-term nature of meteorological, oceanographic and glaciological observations (Jones *et al.*, 2016), and thus establishing the long-term trajectory for Antarctic sea ice on the background of accelerated ice sheet loss remains a challenge. Marine sediment cores provide a longer-term perspective and highlight a major baseline shift in East Antarctic coastal sea ice ~4.5 ka ago (Steig *et al.*, 1998; Crosta *et al.*, 2008; Denis *et al.*, 2010) which characterizes the mid-Holocene 'Neoglacial' transition in the Antarctic. A mechanistic driver for this climate shift currently

remains unresolved, but we propose that two interrelated aspects of the last deglaciation are significantly underrepresented in current models of this transition: (i) the retreat of grounded ice sheets from the continental shelves of Antarctica, and (ii) the subsequent development of large ice shelf cavities during the Holocene. Both factors would significantly alter water mass formation on Antarctica's continental shelves, which today are major source regions of Antarctic Bottom Water (AABW) and Antarctic Surface Water (AASW). These interrelated processes are underrepresented in coupled ocean-atmosphere models which currently do not simulate the timing, magnitude and rapid onset of the Neoglacial (Supplementary Materials).

Integrated Ocean Drilling Program (IODP) Expedition 318 cored a 171 m thick deposit of laminated diatomaceous ooze at Site U1357 offshore Adélie Land (Fig. 1), deposited over the past 11,400 years. Here, we present a new Holocene record of glacial meltwater, sedimentary input and local sea ice concentrations from Site U1357 using compound-specific hydrogen isotopes of fatty acid biomarkers (δ^2H_{FA}), terrigenous grain size, natural gamma radiation, biogenic silica accumulation, highly-branched isoprenoid alkenes (HBIs) and Ba/Ti ratios (Fig. 4 and 5).

We interpret δ^2H_{FA} (Fig. 4) fluctuations in Adélie Drift sediments as a record of meltwater input from isotopically-depleted glacial ice. Antarctic glacial ice is highly depleted in ^2H compared to ocean water, thus creating highly contrasting end-member values for the two major H source pools. Grain size, natural gamma radiation (NGR) and terrigenous and biosiliceous mass accumulation rates (MARs) reflect changing sediment delivery either driven via local glacial meltwater discharge or advection of suspended sediment by oceanic currents. The diene/triene HBI ratio is used as a proxy for coastal sea ice presence (Massé *et al.*, 2011). Ba/Ti enrichment is considered to reflect enhanced primary productivity. These records allow a unique opportunity to reconstruct the magnitude of the coupled response of the ocean and ice sheet during the Neoglacial transition. Details on all proxies and associated uncertainties can be found in Section S2 of the Supplementary Information.

3. MATERIALS AND METHODS

3.1 Organic geochemical analyses

3.1.1 Fatty acid extraction

Lipid extraction of sediment samples was performed at the Royal Netherlands Institute for Sea Research (NIOZ). Freeze-dried and homogenized samples were extracted by Dionex™ accelerated solvent extraction (DIONEX ASE 200) using a mixture of dichloromethane (DCM)/methanol (MeOH) (9:1, v/v) at a temperature of 100°C and a pressure of 7.6×10^6 Pa (Kim *et al.*, 2010).

Compound separation was undertaken at University of Glasgow, UK. The total lipid extract was separated over an aminopropyl silica gel column and the total acid fraction was eluted into an 8ml vial with 4% acetic acid in ethyl-ether solution (Huang *et al.*, 1999). Derivatisation to Fatty Acid Methyl Esters was achieved by adding 200 μl of MeOH containing 14% v/v Boron triflouride to the 8ml vial containing the TAF. FAMES were recovered and cleaned up by eluting through a pre-cleaned 3cm silica gel column (60 A; 35-70) with 4ml of hexane and 4ml of DCM (containing the FAMES). δ^2H values indicate depletion against the international standards: Vienna Pee Dee Belemnite (V-PDB) is the standard for δ13C and Vienna Standard Mean Ocean Water (V-SMOW) for δ^2H.

3.1.2 Fatty acid hydrogen isotope analysis

Compound specific hydrogen isotope analyses of FAMES was performed at the Institute of Low Temperature Science, Hokkaido University. δ^2H values were obtained using a CS-IRMS system with a HP 6890 gas chromatograph and a ThermoQuest Finnigan MAT Delta Plus XL mass spectrometer. Separation of the FAMES was achieved with a HP-5 MS fused silica capillary column (30 m x 0.32 mm i.d., film thickness of 0.25 μm) with a cooled on-column injector. An *n*-alkane and a reference gas whose isotopic values were known was co-injected with the samples as an internal isotopic standard for δ^2H. A laboratory standard (Mix F8 of FAMES from Indiana University) containing C_{10}–C_{30} FAMES was analyzed daily to check the accuracy and the drift of the instrument and to normalize the data to the SMOW/SLAP isotopic scale. The H^{3+} factor was measured every three days.

3.1.3 HBIs

Highly branched isoprenoids (HBI) alkenes were extracted at Laboratoire d'Océanographie et du Climat: Experimentations et Approches Numériques (LOCEAN), separately from the fatty acids, using a mixture of 9mL CH_2Cl_2/MeOH (2:1, v:v) to which 7 hexyl nonadecane (m/z 266) was added as an internal standard, following the Belt et al. (2007) and Massé et al. (2011) protocols. Several sonication and centrifugation steps were applied in order to properly extract the selected compounds (Etourneau *et*

122   *al.*, 2013). After drying with N_2 at 35°C, the total lipid extract was fractionated over a silica column into

123   an apolar and a polar fraction using 3 mL hexane and 6 mL CH_2Cl_2/MeOH (1:1, v:v), respectively. HBIs

124   were obtained from the apolar fraction by the fractionation over a silica column using hexane as eluent

125   following the procedures reported by Belt *et al.* (2007; Massé *et al.*, 2011). After removing the solvent

126   with N_2 at 35°C, elemental sulfur was removed using the TBA (Tetrabutylammonium) sulfite method

127   (Jensen *et al.*, 1977; Riis and Babel, 1999). The obtained hydrocarbon fraction was analyzed within an

128   Agilent 7890A gas chomatograph (GC) fitted with 30 m fused silica Agilent J&C GC column (0.25 mm

129   i.d., 0.25 µm film thickness), coupled to an Agilent 5975C Series mass selective detector (MSD).

130   Spectra were collected using the Agilent MS-Chemstation software. Individual HBIs were identified on

131   the basis of comparison between their GC retention times and mass spectra with those of previously

132   authenticated HBIs (Johns *et al.*, 1999) using the Mass Hunter software. Values are expressed as

133   concentration relative to the internal standard.

134

135   **3.2 Inorganic geochemical analysis and electronic microscopy**

136   Major element concentrations were obtained using X-Ray Fluorescence Scanner on 412 analyses

137   measured directly over undisturbed sediment sections. The bulk major element composition included in

138   this study was measured between sections U1357B-1H-2 to U1357-19H-5 continuously each 50 cm. We

139   used an Avaatech X-ray fluorescence (XRF-Scanner) core scanner at the IODP-Core Repository/Texas

140   A&M University laboratories (USA) during December 2010. Non-destructive XRF core-scanning

141   measurements were performed over 1 cm^2 area with slit size of 10 mm, a current of 0.8 mA and

142   sampling time of 45 seconds at 10 kV in order to measure the relative content of titanium (Ti) and

143   barium (Ba).

144

145   Field emission scanning electron microscopy (FESEM) images and corresponding spectrum were

146   obtained with an AURIGA FIB-FESEM Carl Zeiss SMT at Centro de Instrumentación Científica,

147   Granada University, Spain

148

149   **3.3 Grain size analyses**

150   A total of 341 samples were prepared for grain size analysis. Samples were treated for removal of

151   biogenic opal with a 1M sodium hydroxide NaOH solution and incubated in a water bath at 80°C for 24

152   hours. This procedure was repeated twice due to an incomplete dissolution of diatoms observed in smear

153   slides. The samples were then treated with H_2O_2 to remove organic material at 80°C for 24 hours.

154   Samples were measured using a Beckman Coulter LS 13 320 Laser Diffraction Particle Size Analyser

155   (LPSA). Prior to grain size analysis, ~30 mL of 0.5 g/L Calgon (sodium hexametaphosphate) was added

156   to the samples, and sonicated and stirred in order to disperse the grains and prevent clumping.

157

3.4 Biogenic silica

159   Biogenic silica concentrations (wt% BSi) were measured on 349 discrete samples using a molybdate

160   blue spectrophotometric method modified from (Strickland and Parsons, 1970; DeMaster, 1981).

161   Analytical runs included replicates from the previous sample group and from within the run, and each

162   run was controlled by 10 standards and a blank with dissolved silica concentrations ranging from 0 µM

163   to 1200 µM. For each analysis, ~7 mg of dry, homogenized sediment was leached in 0.1M NaOH at

164   85°C, and sequential aliquots were collected after 2, 3, and 4 hours. Following addition of reagents,

165   absorbance of the 812 nm wavelength was measured using a Shimadzu UV-1800 spectrophotometer.

166   Dissolved silica concentration of each unknown was calculated using the standard curve, and data from

167   the three sampling hours were regressed following the method of DeMaster (1981) to calculate wt%

168   BSi. In our U1357B samples, wt% BSi ranges from maximum of ~60% in early and mid-Holocene light

169   laminae to a minimum of 31% in late Holocene dark laminae. The average standard deviation of

170   replicate measurements is 0.5%.

171

3.5 Model simulations

173   All numerical calculations were performed using the Massachusetts Institute of Technology general

174   circulation model (MITgcm) (Marshall *et al.*, 1997); a three-dimensional, ocean sea-ice, hydrostatic,

175   primitive equation model. The experiments presented here were integrated on a global domain projected

176   onto a cube-sphere grid to permit a relatively even grid spacing and to avoid polar singularities (Adcroft

177   *et al.*, 2004; Condron and Winsor, 2012). The ocean grid has a mean, eddy-permitting, horizontal grid

178   spacing of 1/6° (18-km) with 50 vertical levels ranging in thickness from 10m near the surface to

179   approximately 450m at the maximum model depth. The ocean model is coupled to a sea-ice model in

180   which ice motion is driven by forces generated by the wind, ocean, Coriolis force, and surface elevation

181   of the ocean, while internal ice stresses are calculated using a viscous-plastic (VP) rheology, as

182   described in Zhang and Hibler (1997). In all experiments, the numerical model is configured to simulate

183   present-day (modern) conditions: Atmospheric forcings (wind, radiation, rain, humidity etc.) are

prescribed using 6-hourly climatological (1979-2000) data from the ERA-40 reanalysis product produced by the European Centre for Medium-range Weather Forecasts and background rates of runoff from the ice sheet to the ocean are based on the numerical ice sheet model of Pollard and Deconto (2016) integrated over the same period (1979-2000). To study the pathway of meltwater in the ocean, additional fresh (i.e. 0 psu) water was released into the surface layer of the ocean model at the grid points closest to the front of the Ross Ice Shelf. Five different discharge experiments were performed by releasing meltwater into this region at rates of 0.01 Sv (Sv = 10^6 m3/s), 0.05 Sv, 0.1 Sv, 0.5 Sv, and 1 Sv for the entire duration of each experiment (~3.5 years).

4. ENVIRONMENTAL SETTING AND INTERPRETATION OF PROXY DATA

We utilize a 180 m thick sediment core that was recovered from the Wilkes Land Margin continental shelf in the Adélie Basin (IODP Site U1357). This core targeted an expanded sediment drift (Adélie Drift) and provides a high-resolution Holocene record of climate variability. Below we provide pertinent details on this unique site and on our application of compound specific δ^2H measurements on algal biomarkers as a novel meltwater proxy. Further details on proxy interpretation (Ba/Ti, grain size, HBIs) are given in the Supplementary Materials.

4.1 The Adélie Drift

Site U1357 is located in the Dumont d'Urville Trough of the Adélie Basin, ca. 35 km offshore from Adélie Land (66°24.7990'S, 140°25.5705'E; Fig 1). This is a >1000 m deep, glacially scoured depression on the East Antarctic continental shelf, bounded to the east by the Adélie Bank. Further east lays the Adélie Depression and the Mertz Bank, the latter located north of the Mertz Glacier floating ice tongue. The Adélie Land region is dissected by several glaciers which could potentially contribute terrigenous sediment into the coastal zone with the core site located 40 km to the north of the Astrolabe Glacier, and ca. 75 and 300 km northwest of the Zélée and Mertz glaciers, respectively.

The site itself is located within the Dumont d'Urville polynya (DDUP), which has a summer (winter) extent of 13,020 km^2 (920 km^2), but is also directly downwind and downcurrent of the much larger and highly productive Mertz Glacier polynya (MGP) to the east, with a summer (winter) extent of 26,600 km^2 (591 km^2) (Arrigo and van Dijken, 2003). The MGP forms as a result of reduced sea-ice westward advection due to the presence of the Mertz Glacier Tongue (Massom *et al.*, 2001) and strong katabatic

215 winds which blow off the Antarctic ice sheet with temperatures below -30°C (Bindoff *et al.*, 2000).

216 Katabatic winds freeze the surface waters and blow newly formed ice away from the coast, making the

217 polynya an efficient sea-ice 'factory', with higher rates of sea-ice formation in comparison to non-

218 polynya ocean areas which undergo seasonal sea ice formation (Kusahara *et al.*, 2010). The MGP

219 produces 1.3% of the total Southern Ocean sea ice volume despite occupying less than 0.1% of total

220 Antarctic sea ice extent (Marsland *et al.*, 2004).

221

222 As a result of the upwelling polynya environments, the area along the Adélie Coast is characterized by

223 extremely high primary productivity, with the water column known to host significant amounts of

224 phytoplankton, dominated by diatoms (Beans *et al.*, 2008). The Mertz Glacier zone is generally

225 characterized by stratified waters in the summer, due to seasonal ice melt, with these conditions

226 corresponding to the highest phytoplankton biomass. The lack of ice cover means polynyas are the first

227 polar marine systems exposed to spring solar radiation, making them regions of enhanced biological

228 productivity compared to adjacent waters. A considerable amount of resultant sedimentation is focused

229 via the westward flowing currents from both of these polynyas within the deep, protected Adélie Basin,

230 resulting in a remarkably high sedimentation rate of ca. 1.5-2 cm year^{-1} at Site U1357 (Escutia *et al.*,

231 2011).

232

233 Although biogenic and terrigenous sediment is interpreted to be sourced locally in the Adélie Land

234 region, the mass accumulation rate of these sediments in this drift is associated with the intensity of

235 westward flowing currents (S2.2). Critically, these westward currents also act to transport water masses

236 from further afield, and Site U1357 is directly oceanographically downstream of the Ross Sea, meaning

237 the continental shelf in this region receives significant Antarctic Surface Water (ASSW) transported by

238 the Antarctic Slope Current (ASC) and Antarctic Coastal Current from the Ross Sea embayment . Thus,

239 changes in the surface waters of the Ross Sea influence Site U1357. Whitworth et al. (1998) confirm the

240 continuity of the westward flowing ASC between the Ross Sea and the Wilkes Land margin. This flow

241 is largely associated with the Antarctic Slope Front, which reflects the strong density contrast between

242 AASW and Circumpolar Deep Water (CDW). McCartney and Donohue (2007) estimate that the

243 transport in the westward ASC, which links the Ross Sea to the Wilkes Land margin, reaches 76 Sv (Sv

244 $= 10^6$ m^3 s^{-1}). However, Peña-Molino et al. (2016) measured a highly variable ASC flow at 113°E

245 ranging from 0 to 100 Sv with a mean of -21.2 Sv. This contributes to a cyclonic gyre, which together

246 with the ASC dominate the circulation at Site U1357. The gyre transport is around 35 Sv, and comes

247 mainly from the Ross Sea region, with a lesser contribution from a westward flow associated with the

248 Antarctic Circumpolar Current (McCartney and Donohue, 2007).

249

4.2 Site specific interpretation of $\delta^2 H_{FA}$ as a glacial meltwater proxy

251

4.2.1. Source of fatty acids

253 To best interpret the hydrogen isotope signal recorded by the C_{18} FA, it is important to determine the

254 most likely source these compounds are derived from, and thus the habitat in which they are produced.

255 The C_{18} FA, however, is known to be produced by a wide range of organisms and so we cannot preclude

256 the possibility of multiple sources, especially in a highly diverse and productive region such as the

257 surface waters of offshore Adélie Land. However, we can attempt to determine the most dominant

258 producer(s), which will help us understand the main signal being recorded by the isotopes.

259

260 An analysis of the FAs within eight classes of microalgae by Dalsgaard *et al.* (2003) (compiling results

261 from multiple studies) showed *Cryptophyceae, Chlorophyceae, Prasinophyceae* and *Prymnesiophyceae*

262 to be the most dominant producers of total C_{18} FAs. The *Bacillariophyceae* class, on the other hand,

263 which includes the diatoms, were found to produce only minor amounts of C_{18} FA, instead synthesizing

264 abundant $C_{16:1}$ FAs. Thus, despite the water column offshore Adélie Land being dominated by diatoms,

265 these are unlikely to be a major source of the C_{18} FA within U1357B (Beans *et al.*, 2008; Riaux-Gobin

266 *et al.*, 2011).

267

268 Of the four microalgae classes dominating C_{18} production (Dalsgaard *et al.*, 2003), species from the

269 Chlorophyceae and Prymnesiophyceae classes have been observed within surface waters offshore

270 Adélie Land after spring sea-ice break-up (Riaux-Gobin *et al.*, 2011). Here, *Phaeocystis antarctica* of

271 the Prymnesiophytes was the most abundant of the surface water phytoplankton community

272 (representing 16% of the phytoplankton assemblage), whereas Cryptophyceae spp. were found in only

273 minor abundances (Riaux-Gobin *et al.*, 2011). In the Antarctic, *Phaeocystis* is thought to be the most

274 dominant producer of C_{18} FAs (Dalsgaard *et al.*, 2003), and thus is likely to be a key producer of the C_{18}

275 FA in U1357B samples.

276

277　To investigate this further, we measured compound-specific carbon isotopes of the C_{18} FAs in U1357B

278　samples, which gives an average $\delta^{13}C$ value of -29.8 ± 1.0 ‰ (n=85). Budge *et al.* (2008) measured a

279　similar $\delta^{13}C$ value of -30.7 ± 0.8‰ from C_{16} FAs derived from Arctic pelagic phytoplankton, while sea

280　ice algae and higher trophic level organisms all had much higher $\delta^{13}C$ values (sea ice algae having

281　values of -24.0 ± 2.4‰). Assuming similar values apply for the C_{18} FA and for organisms within the

282　water column at our site, this suggests that our C_{18} FA is predominantly derived from pelagic

283　phytoplankton.

284

285　Furthermore, $\delta^{13}C$ measurements of suspended particulate organic matter (SPOM) near Prydz Bay, East

286　Antarctica by Kopczynska *et al.* (1995) showed that sites with high $\delta^{13}C$ SPOM values (-20.1 to -

287　22.4‰) were characterized by diatoms and large heterotrophic dinoflagellates, whereas the lowest $\delta^{13}C$

288　SPOM values (-29.7 to -31.85‰) were associated with *Phaeocystis*, naked flagellates and autotrophic

289　dinoflagellates. Wong and Sackett (1978) measured the carbon isotope fractionation of seventeen

290　species of marine phytoplankton and showed that Haptophyceae (of which *Phaeocystis* belongs) had the

291　largest fractionation of -35.5‰.

292

293　Therefore, based on the known producers of C_{18} FAs, observed phytoplankton assemblages within

294　modern surface waters offshore Adélie Land, and the $\delta^{13}C$ value of C_{18} FAs in U1357B samples, as

295　discussed above, we argue that the C_{18} FA here is predominantly produced by *Phaeocystis* (most likely

296　*P. antarctica*), but with potential minor inputs from other algal species such as Cryptophytes or diatoms.

297

298　*Phaeocystis antarctica* is a major phytoplankton species within the Antarctic, dominating spring

299　phytoplankton blooms, particularly in the Ross Sea (DiTullio *et al.*, 2000; Schoemann *et al.*, 2005). It is

300　known to exist both within sea ice and in open water (Riaux-Gobin et al., 2013) and has been observed

301　in surface waters in great abundance following spring sea-ice break-up, at both coastal and offshore sites

302　in Adélie Land (Riaux-Gobin *et al.*, 2011).

303

304　Although a large proportion of organic matter produced in the surface water is recycled in the upper

305　water column, the small fraction which is deposited in the sediment reaches the sea floor through large

306　particles sinking from above as "marine snow". This export production includes large algal cells, fecal

307　pellets, zooplankton carcasses and molts, and amorphous aggregates (Mayer, 1993). In the Ross Sea,

aggregates of *P. antarctica*, have been observed to sink at speeds of more than 200 m day^{-1}, meaning they could reach deep water very quickly (Asper and Smith, 1999). In this way, a proportion of the lipid content of *P. antarctica* and other algae is transported and sequestered in the sediments.

Initial diagenesis is characterized by the preferential degradation of more labile organic compounds e.g. sugars, proteins, amino acids. Proportionally, lipids are relatively recalcitrant compared to other compounds (e.g. amino acids, proteins) and thus are more likely to be preserved as molecular biomarkers on geological timescales, even where the rest of the organism may be completely degraded (Peters and Moldowan, 1993). The final proportion of lipids that are preserved within sediments are affected by factors including the export production, O_2 content, residence time in the water column and at the sediment/water interface before deposition, molecular reactivity, formation of macromolecular complexes, adsorption to mineral surfaces and bioturbation (Meyers and Ishiwatari, 1993; Killops and Killops, 2004). Within lacustrine sediments, a significant shift in FA distributions has been shown to occur within 100 years due to early diagenesis, after which the FA distribution remains relatively unaffected by diagenesis (Matsuda, 1978), thus major changes are assumed to reflect primary environmental signals on longer timescales such as in our Holocene record. Due to the hyperproductivity of the surface waters offshore Adélie land, we assume the dominant inputs of the C_{18} FA are from algal sources in overlying waters and upcurrent regions. Allochthonous inputs e.g. long-range aeolian transport of plant material are assumed to be minimal.

4.2.2. Interpretation of hydrogen isotopes

Compound-specific H isotopes of algal biomarkers are a well-used climate proxy in sediments throughout the Cenozoic (e.g. Pagani *et al.*, 2006; Feakins *et al.*, 2012). Although diagenetic alteration, including H-exchange, is possible within sedimentary archives, this has shown to be minimal in sediments younger than 20 Ma (Sessions *et al.*, 2004). Furthermore, if H-exchange had occurred, we would expect δ^2H values between different FA chain lengths and closely spaced samples to be driven towards homogeneity, yet large variability remains, suggesting this is not the case. Thus, we are confident that our measured H isotopes are indicating a primary signal throughout the Holocene.

337   The δ^2H value preserved in biomarkers is known to be correlated, but offset, with the δ^2H of the water

338   from which the hydrogen was derived. Measured δ^2H can therefore be described as a function of either

339   the δ^2H of the water source, or the fractionation occurring between source water and the lipid ($\varepsilon_{l/w}$) (i.e.

340   vital effects), in which various environmental factors play a part (Sachse *et al.*, 2012).

341

342   The main environmental factors controlling $\varepsilon_{l/w}$ are salinity and temperature, with which δ^2H increases

343   by 1-4‰ per increase in practical salinity unit (psu) (Schouten *et al.*, 2006; Sachse *et al.*, 2012) and

344   decreases by 2-4‰ per degree C increase (Zhang *et al.*, 2009), respectively. The δ^2H$_{FA}$ record from Site

345   U1357 displays an absolute range of ca. 123‰, and millennial to centennial scale variability with an

346   amplitude of ca. 50‰, throughout the core. This would imply extremely large and pervasive variations

347   in temperature (up to ca. 60°C) and salinity (up to 123 psu) if fractionation driven by either of these

348   factors were the main control. One study has shown the salinity of present day Adélie shelf waters to

349   vary between 34 and 34.8 psu (Bindoff *et al.*, 2000), while tetraether-lipid based subsurface (50-200 m)

350   temperature estimates from nearby Site MD03-2601 (about 50 km west of Site U1357) range from -0.17

351   to 5.35°C over the Holocene (Kim *et al.*, 2010). Therefore, fractionation changes driven by temperature

352   or salinity cannot be invoked as a major control on δ^2H$_{FA}$ in the Holocene.

353

354   Thus, the most parsimonious explanation relates to changes in δ^2H$_{FA}$ of the water source (Sachse *et al.*,

355   2012). In the Adélie Basin, the most apparent controls on this are advection, upwelling or inputs of

356   isotopically depleted glacial meltwater. The δ^2H$_{FA}$ value within Antarctic glaciers is highly depleted

357   relative to sea water due to the Rayleigh distillation process, leading to highly negative isotope values

358   for precipitation over the continent.

359

360   The glacial meltwater originating from the Ross Ice Shelf is likely to combine ice precipitated

361   throughout the Holocene and glacial period, and from both the East and West Antarctic Ice Sheets.

362   However, as noted by Shackleton and Kennett (1975) in their first oxygen isotope record of the

363   Cenozoic (see their Fig. 6), most of the ice that melts around the margin has been coastally precipitated

364   (due to higher accumulation rates). Since ice precipitated further inland has a greater residence time

365   (Shackleton and Kennett, 1975) and significantly lower accumulation rates it will contribute

366   significantly less to this signal. Thus, the ice that was melting along this margin is best represented by

367   average values of coastal ice dome records at a similar latitude to that which melted since the LGM

368 (such as TALDICE and Siple Dome) than more southerly locations. Glacial to Holocene δ^2H_{FA} values

369 from TALDICE, located on the western edge of the Ross Sea in the East Antarctic, for example, vary

370 between -276.2 and -330.3‰ (Steig *et al.*, 1998) (converted from $\delta^{18}O$ values following the global

371 meteoric water line (GMWL): $\delta^2H_{FA} = 8.13 \ (\delta^{18}O) + 10.8$), while values from Siple Dome on the

372 eastern edge of the Ross Sea in the West Antarctic, vary from ca. -200 to -293‰ (Brook *et al.*, 2005).

373 Taking the average of these values as an approximate estimate for the meltwater gives a δ^2H value of ca.

374 -275‰. We note our calculations are based on averages of set time periods, which we expect would

375 integrate ice of various ages - rather than extreme values which could relate to specific melt events of ice

376 or biases to certain ages/regions. This seems reasonable - the isotopic signal of coastal surface waters

377 masses advected from the RIS to the Adélie land (as illustrated in Fig. 2 and 3) must integrate a range of

378 source areas across the RIS and from the coast around to Adélie Land.

379

380 In comparison to the highly negative glacial ice isotope composition, sea surface water $\delta^{18}O$

381 measurements taken near the Mertz Glacier offshore Adélie Land (140-150°E) in summer 2000-2001

382 ranged between -0.47 and 0.05‰ (Jacobs *et al.*, 2004), equivalent to δ^2H values of 6.9 to 11.2‰

383 (average = 9‰) following the GMWL. Thus, the two major hydrogen source pools (RIS glacial ice and

384 ocean water) have highly contrasting isotope values, meaning inputs of upstream glacial ice could have a

385 large effect on surface water δ^2H values in the Adélie Land region.

386

387 Taking the average glacial meltwater δ^2H value as -275‰ and the average modern Adélie surface water

388 δ^2H value of 9‰ as end-members, and assuming a biosynthetic offset between the FA and sea water of

389 173‰ (see below), we can use a simple mixing model to estimate the percentage of glacial meltwater

390 required in the surface waters to change the δ^2H_{FA} value to those recorded in U1357B samples. The

391 most negative values occur during the early Holocene, 11.4 – 8.2 ka, averaging -214.2‰ (n=18) which,

392 converted to a surface water value of -41‰, requires 17.6% of the surface water to be comprised of

393 glacial meltwater. During this time, we argue that large volumes of meltwater were reaching the core

394 site as local glaciers retreated, leading to intense surface-water stratification. Thus, a relatively high

395 percentage of meltwater in the Adélie Land surface waters seems reasonable. During the mid-Holocene

396 (5-4 ka), the average δ^2H_{FA} is very similar (-213.9‰, n=7), requiring 17.2% of the surface water to be

397 derived from glacial meltwater. During this time, we argue for the dominant meltwater source as coming

398 from the Ross Sea, and interpret this as a major period of glacial retreat (see section 5.2), during which

399 large volumes of meltwater are injected into the surface water and transported to the Adélie coast. In

400 contrast, the most recent samples (last 0.5 ka, n=7), which includes the most positive value of the record,

401 has an average δ^2H $_{FA}$ value of -174.5‰. This brings the surface water value up to -1.5‰, which

402 approaches modern measured values, and requires just 3.7% (e.g. well within uncertainties) of the

403 surface waters in the Adélie Land to be glacial meltwater. However, it is also possible that the meltwater

404 was dominated by more LGM-aged ice. In either case, perturbation of the exact isotopic values still

405 indicate only significant changes in the flux of glacial meltwater can account for this signal. For

406 example, the use of -330‰ (LGM values) for the ice input gives an estimate of 3% of the surface water

407 being comprised of glacial meltwater for latest Holocene values, and 14.7% for pre 8 ka values. Taking -

408 240‰ (Holocene values) for the ice input gives an estimate of 4% for latest Holocene values, and 20%

409 for pre 8 ka values). Thus even with changing isotopic values though the deglacial, this signal of

410 changing meltwater flux would still dominate. We note these are semi-quantitative estimates, as the

411 salinity and temperature fractionation could reduce these estimates further (but salinity and temperature

412 can only ever account for a small part of the signal).

413

414 Surface water $\delta^{18}O$ values around Antarctica (below 60°S), measured between 1964 and 2006, ranged

415 from -8.52‰ to 0.42‰ (Schmidt *et al.*, 1999), the most negative value having been measured proximal

416 to the George VI Ice Shelf edge, where high melt rates have been observed (Potter and Paren, 1985). If

417 converted to δ^2H using the global meteoric water line, these values give a δ^2H range of 83.4‰. Thus,

418 our absolute δ^2H_{FA} range of 123‰ over the Holocene suggests a range of isotopically depleted

419 meltwater inputs to our core site over this time that are 1.5 times greater than that occurring in different

420 locations around the Antarctic in recent decades. This seems plausible based on geological evidence that

421 indicates large glacial retreat and ice mass loss occurred from the Ross Sea sector during the Holocene

422 (Anderson et al., 2014; McKay *et al.*, 2016; Spector et al., 2017), meaning resultant changes in surface

423 water are likely to be greater in magnitude than observed around the Antarctic in recent decades. This

424 assumes a relatively constant value for the isotopic composition of glacial meltwater, however, there is

425 likely to be some variability due to the possibility of melting ice of different δ^2H values. But, as

426 discussed above, the meltwater is best represented by the average values of the ice sheet, rather than

427 extreme values, since it must (over the broad expanse of the RIS) include an integrated signal, and thus

428 the actual variation in meltwater δ^2H will be significantly within the range of the end-members.

429

430   Although the biosynthetic fractionation of the C_{18} FAs in U1357B is unknown, we assume that the offset

431   with surface water remains relatively constant throughout the record. Sessions *et al.* (1999) showed the

432   biosynthetic fractionation of hydrogen isotopes in the C_{18} FA from four different marine algae to range

433   from -189 to -157‰. If we take the average of these values of 173‰ and apply this as a biosynthetic

434   offset to the youngest samples in U1357B (last 0.5 ka, n=7), which includes the most positive value of

435   the record, gives an average $\delta^2 H_{FA}$ value of -174.5‰. This brings the surface water value up to -1.5‰,

436   which approaches modern measured values (Jacobs *et al.*, 2004).

437

438   Furthermore, it is interesting to note that the biosynthetic offsets measured by Sessions *et al.* (1999) for

439   the C_{18} FA from different algal species have a total $\delta^2 H$ range of 32‰. Although we cannot dismiss

440   changes in the relative contribution of C_{18} from different species in U1357B samples (and thus different

441   biosynthetic fractionations), we argue this would only be a minor control on $\delta^2 H$ compared to other

442   influences. As a thought experiment, taking the above end-members for biosynthetic fractionation from

443   Sessions *et al.* (1999), even with a 100% change in C_{18} producer to a different algal source, this could

444   only explain a quarter of the observed $\delta^2 H$ change (i.e. 32‰ of 123‰).

445

446   Therefore, we interpret the first order control on $\delta^2 H_{FA}$ at Site U1357 as inputs of isotopically depleted

447   glacial meltwater. Such inputs are, in turn, influenced by the mass balance of the proximal or up-current

448   glaciers and ice-shelves.

449

450   **4.3 Other proxies**

451   Grain size, natural gamma radiation (NGR) and terrigenous and biosiliceous mass accumulation rates

452   (MARs) reflect changing sediment delivery either driven via local glacial meltwater discharge or

453   advection of suspended sediment by oceanic currents. The diene/triene HBI ratio is used as a proxy for

454   coastal sea ice presence (Massé *et al.*, 2011), in which high values indicate greater sea ice extent over

455   the core site. The HBI diene, also known as Ice Proxy for the Southern Ocean with 25 carbon atoms

456   (IPSO25), has been shown to derive from a sea-ice associated diatom (Belt et al., 2016), whereas the

457   HBI triene is produced in the marginal ice zone (Smik et al., 2016). Ba/Ti enrichment is considered to

458   reflect enhanced primary productivity. Interpretation of these proxies is discussed in more detail in

459   Supplementary Information S2.

5 RESULTS

5.1. Model simulations

We employed a series of sensitivity tests from a high-resolution numerical ocean model by releasing a range of meltwater volumes (0.01 to 1 Sv) from along the front of the Ross Ice Shelf (RIS) to determine its pathway. This demonstrates that, even under the lowest flux scenarios, freshwater is transported anticlockwise, entrained within the coastal current (Fig. 2 and 3), and reaches Site U1357 within a year. Moreover, although the higher input scenarios are not realistic values for the release of meltwater since the LGM, the full range of simulations show a strong linear relationship between meltwater flux and salinity change at the core site (Fig 3), suggesting the magnitude of the signal recorded at Site U1357 is directly related to the magnitude of meltwater released. Thus, we argue that any changes in Ross Sea water mass properties (salinity and temperature) would have a direct influence on surface water mass properties at Site U1357 during the Holocene.

5.2 Geochemical data

The main datasets from Core U1357 are displayed in Fig 4 and 5. FA δ2H (Fig 4a) shows and overall trend towards more positive values over the course of the Holocene, indicating a decline in glacial meltwater input. There is a notable deviation from this trend in the mid-Holocene involving a sustained period of more negative δ2H values, suggesting a peak in meltwater input, centred on ca. 4.4 ka. This mid-Holocene deviation in FA δ2H coincides with an increase in the HBI diene/triene ratio (Fig. 4c), indicating a baseline shift in sea ice conditions whereby greater sea ice concentrations are sustained for the rest of the Holocene. This is a similar pattern to the relative abundance of the *Fragilariopsis curta* group (Fig 4b), a sea ice diatom group in core MD03-2601 also indicating a shift in sea ice concentrations. Along the entire record, Ba/Ti ratios show persistent periodic fluctuations in marine productivity, with values between 0.1 and 2.7 (Fig. 4g). A marked enrichment can be observed at ca. 4.4 ka reaching Ba/Ti ratio values over 36.1, suggesting a peak in primary productivity, before declining to background levels again (Fig. 4).

5.3 Sedimentological data

The stratigraphy of U1357B is divided into three units: the lowermost 10 cm recovered Last Glacial Maximum (LGM) till (Unit III), overlain by 15 m of laminated mud-rich diatom oozes with ice rafted debris (IRD) (Unit II), and the upper most 171 m (Unit I) consists of laminated diatom ooze with a general lack of IRD and a significant reduction in terrigenous sediment (Escutia *et al.*, 2011).

Between ca. 11.4 and 8 ka, U1357B has a relatively high terrigenous component (i.e. high Natural Gamma Radiation (NGR) content and low BSi%; Fig 5). The grain size distribution contains coarse tails of fine (125-250 μm) to medium sands (250-500 μm), but only one sample contains coarse sands (>500 μm) that may represent ice-berg rafted debris (IBRD). However, terrigenous content and IBRD is more common in the underlying Unit II. The fine-grained sands and muds have a distribution with similar modes to overlying intervals, albeit with an increase in the size of the coarse silt and very fine sand modes. There is a subtle increase in sorting up core between ca. 11.4 and ca.8 ka (from very poorly to poorly sorted, Fig. 5).

Between 9 and 4.5 ka, mass accumulation rates (MARs) (both biogenic and terrigenous; Fig. 5) are relatively high, albeit with millennial scale variability. However, the mean grain size and sorting of the terrigenous material is relatively stable throughout the entire interval, and as with the rest of Unit I there is an almost complete lack of IBRD. There is a rapid increase in mud content at 4.5 ka coincident with a reduction in both the biogenic and terrigenous MARs, although the terrigenous MAR curve shows higher accumulation rates than the biogenic MAR curve (Fig. 5).

6 DISCUSSION

The sedimentology and geometry of the drift prior to ~11.4 ka (Unit II) is consistent with the calving bay re-entrant model (Domack *et al.*, 2006; Leventer *et al.*, 2006) (Fig. 1 and Supplementary Fig. S4; Supplementary Materials), whereby LGM ice retreated in the deeper troughs while remaining grounded on shallower banks and ridges. Sediment laden meltwater and IRD content in Unit II (>11.4 ka) is thus likely derived from local outlet glaciers. However, anomalously old radiocarbon ages due to glacial reworking precludes development of a reliable age model prior to the Holocene (Supplementary Materials).

The results of model simulations (Section 5.1) indicate that, although several small glaciers within Adélie Land may contribute meltwater to the site, the region is also likely to be influenced significantly by changes in Ross Sea waters. Freshwater release simulations from the Ross Ice Shelf (RIS) confirm

518 this oceanographic continuity between the Ross Sea and the Wilkes region (Fig 2). All five simulations

519 indicate that meltwater released from the edge of the RIS is almost completely entrained within the

520 westward coastal surface current and reaches Site U1357 within 4 months to 1 year (Fig 3). These fluxes

521 cover a wide range of meltwater inputs and show a strong linear relationship with salinity at the core site

522 (Fig. 4). This suggests that the magnitude of the signal recorded at Site U1357 is directly related to the

523 magnitude of the meltwater input.

524 Local processes do also play a critical role in this region. For example, episodic calving events of the

525 Mertz Glacier tongue release fast ice over the drill site and create strong surface water stratification,

526 cutting off local AABW production (Campagne *et al.*, 2015). Although appearing to be only a local

527 process, there is still a regional (Ross Sea) influence, as this fast ice that builds up behind the Mertz

528 Glacier is formed by the freezing of fresher AASW transported from the Ross Sea (Fig 2). Thus,

529 conditions in the Ross Sea, such as the melting of isotopically depleted glacial ice, would influence both

530 the isotopic composition and amount of this sea ice.

531

532 **6.1 Early Holocene**

533 The base of the drift deposit shows down-lapping of material suggesting a supply from the south,

534 indicating local focusing of meltwater and terrigenous material was the dominating influence until 11.4

535 ka (Supplementary Materials). This is overlain by onlapping strata (Unit I) with the drift forming an

536 east-west elongation on the northern flank of the Dumont d'Urville Trough, which is more consistent

537 with advection of material from the east than with delivery from local outlet glaciers to the south. Thus,

538 an increased meltwater influence from the Ross Sea is likely since this time.

539

540 Due to the potential for competing sources of glacial meltwater in the earliest Holocene, we focus our

541 study on Unit I, where there is less influence of calving bay processes (Escutia *et al.*, 2011). However,

542 the earliest part of Unit I (11.4 to 8 ka BP), which includes the most negative δ^2H_{FA} values, is

543 characterized by a very gradual up-core increase of sorting in the terrigenous sediment supply,

544 decreasing natural gamma ray (NGR) values (Fig. 5) and a general lack of IRD. We conservatively

545 interpret this as potentially maintaining some local glacial meltwater input from local outlet glaciers in

546 the lowermost interval of Unit I. Nevertheless, this process was probably greatly reduced relative to Unit

547   II deposition and it is likely much of this signal between 11.4 and 8 ka could still be derived from water

548   masses advecting to the site from the east (e.g. the Ross Sea).

549

550   This is supported by geological and cosmogenic evidence which demonstrates that the majority of the

551   margin of the East Antarctic, and also the Amundsen Sea margins, had retreated to their modern-day

552   positions by ~10 ka (Bentley et al., 2014; Mackintosh et al., 2014; Hillenbrand et al., 2017). Thus, these

553   margins are unlikely to contribute large scale shifts in meltwater fluxes to the Adélie Coast during most

554   of the Holocene. The history of grounding line retreat in the Ross sea is relatively well-constrained,

555   particularly in the Western Ross Sea, and the loss of residual ice caps appears to be largely complete by

556   ca. 7 ka to the immediate north of Ross Island, near present day calving line front of the Ross Ice Shelf

557   (Anderson et al., 2014; McKay et al. 2016). Indeed, the phase of isotopically depleted glacial meltwater

558   is apparent at Site U1357 between 8 and 7 ka could be sourced from the Ross Sea, reconciling our data

559   with these chronologies. Prior to 8 ka, any meltwater signal in U1357B is potentially influenced by local

560   glacier retreat, based on the caveats noted earlier in the grainsize and geophysical datasets (S2.2),

561   although we note a dominant Ross Sea contribution to this signal is possible.

562

563   Glacial retreat, however, persisted in the Ross Sea until at least 3 ka (Anderson et al., 2014; Spector et

564   al., 2017) providing a large upstream source of meltwater feeding into the Adélie Coast. We therefore

565   interpret our meltwater signal as being dominated by Ross Sea inputs since at least 8 ka, but potentially

566   as early as 11.4 ka. Furthermore, the retreat of grounded ice from the outer Ross Sea continental shelf

567   was accompanied by the growth of a significant floating ice shelf (which was not the case in the

568   Amundsen Sea or proximal East Antarctic coast) (Bentley et al., 2014).

569

570   An overall trend to more positive δ^2H_{FA} values, from the most negative value of the record at ~9.6 ka, to

571   ~8 ka indicates decreasing meltwater (Fig. 4a), thus suggesting a gradually diminished input from either

572   local outlet glaciers or the Ross Sea. This is associated with an increase in MARs, between 10 and 8 ka,

573   and is tentatively interpreted to represent the final retreat of residual ice from local bathymetric highs

574   allowing more material to advect into the drift (Fig. 5). Although there is millennial scale variability,

575   MARs remain relatively high until 4.5 ka. However, δ^2H_{FA} and MARs show greater coherence at the

576   millennial-scale after 7 ka BP, suggesting that increased fluxes of glacial meltwater broadly

577 corresponded to stronger easterly currents, which advected biogenic and terrigenous material into the

578 drift.

579

6.2 Middle Holocene

581 A negative excursion in $\delta^2 H_{FA}$ starting from 6 ka and culminating at 4.5 ka is interpreted to record a

582 period of enhanced glacial meltwater flux to the site relating to a final retreat phase of the major ice

583 sheet grounding line in the Ross Sea embayment (Fig. 6). A marked enrichment of Ba/Ti ratios also

584 occurs at 4.5 ka, reaching values of 36.1, on a background of baseline fluctuations between 0.1 and 2.7

585 (Fig. 4g), which suggests enhanced primary productivity, potentially driven by meltwater-induced

586 stratification. Ongoing Holocene retreat in the Ross Sea is interpreted to be primarily the consequence of

587 marine ice sheet instability processes resulting from the overdeepened continental shelf in that sector

588 (McKay et al., 2016). We use the model presented by Lowry et al. (2019) to help constrain the pattern

589 and rate of retreat of the grounding line to the south of Ross Island. This model compares geological

590 data with ice sheet model experiments that were forced by a range of environmental conditions. These

591 experiments indicate that the Ross Ice shelf cavity only started to expand once the grounding line

592 retreated to the south of Ross Island. Furthermore, to reconcile these model experiments with geological

593 datasets, the cavity expansion was not completed until the mid-Holocene (ca. 5 ka). This reconciles well

594 with [10]Be exposure ages of erratics in coastal nunataks at the confluence of the Mercer Ice Stream and

595 Reedy Glacier indicate 105 m of ice sheet deflation since 6.8 ka, with 40 m of this after 4.9 ka (Todd et

596 al., 2010), indicating the most rapid phase of retreat occurred between 6.8 ka and 4.9 ka. More recent

597 deflation profiles for the Beardmore Glacier (84°S) and Scott Glacier (86°S) regions show sustained

598 thinning between ca. 9 and 8 ka, but the Scott Glacier experience a second phase of rapid thinning of ca.

599 200 m between 6.8 and 5.3 ka (Fig. 4), followed by a slower rate of thinning of between 5.3 and 3.5 ka

600 of ca. 100 m. Ages younger than this, near the modern surface are thought to be related to surface

601 ablation rather than dynamic thinning. This suggests that the grounding line was at its modern location

602 by ca. 3.5 ka (Spector et al., 2017) although it may have potentially retreated further south, followed by

603 a short duration readvance of the grounding line (Kingslake, et al., 2018). Glaciological evidence from

604 radar profiles suggests the development of divide flow on Roosevelt Island occurred sometime between

605 3 and 4 ka BP, suggesting that the ice sheet thickness was at least 500 m thicker until this time (Conway

606 et al., 1999). Combined, these lines of evidence suggest the majority of grounding line retreat south of

607 Ross Island occurred after 8 ka, with a sustained retreat occurring after 6.8 ka, consistent with the timing

608   of the largest inputs of glacial meltwater feeding the U1357 site. However, a younger age (e.g. 3 – 3.5

609   ka) for final establishment of the modern grounding line position is consistent with our interpretation, as

610   although the meltwater signal in δ^2H_{FA} peaks at 4.5 ka, it does not stabilise at lower levels until 3 ka.

611

612   The δ^2H_{FA} peak at 4.5 ka in U1357 coincides directly with a rapid shift in HBI biomarker ratios at the

613   site (Fig. 4a and c), as well as sea ice proxies recorded in nearby site MD03-2601 (Fig. 4b), in the Ross

614   embayment (Taylor Dome ice core on a revised age model) (Steig *et al.*, 1998; Baggenstos *et al.*, 2018)

615   (Fig. 4d) and other sectors of the East Antarctic margin in Prydz Bay (JPC24) (Denis *et al.*, 2010) (Fig.

616   4e), reflecting a widespread increase in coastal sea-ice concentration and duration. We interpret

617   decreasing MAR and finer-grained terrigenous content (e.g. increased mud percent) at Site U1357 after

618   4.5 ka (Fig. 5) to also be a consequence of increased coastal sea ice, reducing wind stress on the ocean

619   surface and limiting the easterly advection of detritus to the drift deposit.

620

621   Coastal sea-ice concentration and duration remain high throughout the rest of the Holocene (this study

622   and Steig *et al.*, 1998; Crosta *et al.*, 2008; Denis *et al.*, 2010), compared to the period before 4.5 ka,

623   despite a decrease in glacial meltwater flux to the U1357 site. In addition, meltwater input prior to 4.5 ka

624   does not have a major influence on sea ice extent. Thus, an increase in meltwater flux cannot explain the

625   Neoglacial intensification of sea ice at ~4.5 ka. Here, we propose that greater coastal sea ice cover since

626   4.5 ka is related to the development of a large ice-shelf cavity in the Ross Sea as the ice sheet retreats

627   (Fig. 6), which pervasively modified ice shelf-ocean interactions and increased sea ice production.

628   Models suggest a large cavity on the continental shelf increases contact between basal-ice and

629   circulating ocean water, driving the formation of a cool, fresh water mass feeding into the AASW,

630   stabilizing the water column and enhancing the production of sea ice (Hellmer, 2004) (Fig. 6). However,

631   under small cavities such as in the modern Amundsen Sea influenced by warm-water incursions, ice

632   shelf melting results in an "ice pump" enhancement of sub-ice shelf circulation. This increases flow of

633   warm Circumpolar Deep Water (CDW) under the ice shelf that is 100-500 times the rate of melt, and

634   this volume of water does not allow for supercooling. Small cavity ice shelf outflows are therefore warm

635   and act to restrict sea ice at the ice shelf front (Jourdain *et al.*, 2017). Thus, during the Holocene, the size

636   of the cavity must have reached a threshold after which this positive warming feedback switched to a

637   negative feedback. We argue that such a tipping point takes place at 4.5 ka BP, when our proxy data

638   suggest meltwater peaks, and would explain why the increase in sea-ice concentration appears rapid and

639 only occurs at the peak of the meltwater input, and not during its prior increase, or previous meltwater

640 inputs (Fig. 4a-g).

641

642 Although the glacial meltwater volume is greatly reduced after 4.5 ka BP, the volume of Ice Shelf Water

643 (ISW) produced beneath the modern RIS is estimated at 0.86 Sv-1.6 Sv (Holland *et al.*, 2003; Smethie

644 and Jacobs, 2005). We note that ISW is not glacial meltwater, but it is defined as a supercooled water

645 mass formed through interaction with the base of the RIS, but once formed acts to modify other water

646 masses in the Ross Sea. A significant proportion of ISW is high salinity and is thus advected northwards

647 at intermediate waters depth to ultimately form AABW. However, a significant volume of ISW is lower

648 salinity and buoyant, due to development of frazil ice, and acts to mixes with surface waters (Robinson

649 *et al.*, 2014). Currently, a 0.4 Sv plume of ISW in the western margin of the Ross Ice Shelf (Robinson *et*

650 *al.*, 2014) is directly delivered to the surface resulting in enhanced sea ice production, while seasonal

651 melt of this enhanced sea ice further acts to cool and freshen surface waters. Although unrealistic in the

652 context of a post-LGM meltwater flux from the Ross Sea alone, the larger meltwater release scenarios in

653 our simulations (0.5 to 1 Sv) show the potential pathways that a cool, fresher surface water mass

654 collecting and forming on the broad Ross Sea continental shelf would follow (Fig. 2). These waters are

655 transported in easterly coastal currents to the Weddell Sea and the Antarctic Peninsula. This eventually

656 retroflects to join the Antarctic Circumpolar Current (Fig. 2b), and thus has potential for cooling and

657 freshening in the South Atlantic far offshore, as the ice shelf cavity increased in the Ross Sea. Indeed,

658 offshore site TTN057-13 records increased lithics in the South Atlantic after 4.5 ka (Fig. 4f), relative to

659 the period before, suggested to have been predominantly transported by sea ice indicating a cooling in

660 sea surface temperatures and increase in sea-ice extent in the South Atlantic at this time (Hodell et al.,

661 2001; Nielsen *et al.*, 2007). However, it also is feasible that this circum-Antarctic cooling signal

662 indicates similar melt processes may have been occurring in the Weddell Sea at ~4.5 ka, as suggested by

663 cosmogenic nuclide data (Hein *et al.*, 2016).

664

665 **6.3 What Drove the Neoglacial Transition?**

666 Our observed coastal sea-ice increase is part of a widespread transition to Neoglacial conditions both

667 globally and at high southern latitudes (Kim *et al.*, 2002; Masson-Delmotte *et al.*, 2011; Marcott *et al.*,

668 2013; Solomina *et al.*, 2015). However, most current climate models do not simulate this cooling trend,

669 resulting in a significant data-model mismatch (Liu *et al.*, 2014) (Supplementary Fig. S6). Marine ice

sheet retreat along the Pacific margin of West Antarctic has previously been proposed to be triggered by enhanced wind-driven incursions of warm CDW onto the continental shelves in the early Holocene (Hillenbrand *et al.*, 2017), with continued retreat in the Ross Sea being the consequence of the overdeepened continental shelf and marine ice sheet instability processes (McKay *et al.*, 2016). We propose that a series of negative feedbacks was also associated with the latter phases of this retreat due to the RIS cavity expansion that occurred in the mid-Holocene, with similar processes possibly occurring in the Weddell Sea, leading to the onset and continuation of Neoglacial conditions. Widespread albedo changes associated with increased coastal sea ice would have amplified regional cooling trends (Masson-Delmotte *et al.*, 2011), whilst increased stratification resulting from seasonal sea-ice melt and increased ISW production drove the deepening of the fresher water surface isopycnal at the continental shelf break. Grounding line retreat creates new space for continental shelf water masses to form, while ice shelf cavity expansion promotes supercooling of waters circulating beneath the ice shelf, and freshening of AASW. Thus, as seasonal sea ice melt and ice shelf supercooling processes played a greater role in enhancing AASW cooling and production on the continental shelf, they would have acted to restrict warmer subsurface water transport onto the continental shelf (Smith Jr. *et al.*, 2012) (Fig. 6). Furthermore, the Neoglacial sea-ice increase itself may have been associated with a stabilising feedback mechanism (which also is not resolved in ice-ocean models) through its role in dampening ocean-induced wave flexural stresses at ice shelf margins, reducing their vulnerability to catastrophic collapse (Massom *et al.*, 2018). We suggest that some combination of the above processes could have acted to slow the rate of Ross Sea grounding line retreat and reduced basal ice shelf melt as indicated by a trend towards more positive $\delta^2 H_{FA}$ values in U1357 between 4.5 and 3 ka (Fig. 4a). Furthermore, large Antarctic ice shelves currently have large zones of marine accreted ice resulting from supercooling (Rignot *et al.*, 2013), thus the signature of $\delta^2 H_{FA}$ is anticipated to become more positive as the ice shelf approaches a steady state of mass balance, relative to the thinning phases when basal melt rates exceed that of accretion. The stabilization of $\delta^2 H_{FA}$ values observed at 3 ka in U1357 suggests the Ross Ice Shelf has maintained a relatively steady state of mass balance since this time.

A recent study implies that the late Holocene shift in patterns of coastal versus open water sea ice patterns in the Ross Sea was driven an increase in katabatic winds since at least 3.6 ka in the Ross Sea (Mezgec *et al.*, 2017), leading to enhanced polynya activity. During colder Antarctic climates, increased latitudinal temperature gradients enhanced katabatic winds in the Ross Sea (Rhodes *et al.*, 2012). This is

consistent with our hypothesis, as we interpret this katabatic wind and polynya activity signal to be a response to the preceding Neoglacial cooling at 4.5 ka and evolution of the modern ocean-ice shelf connectivity, which our data suggest was primarily driven by ice shelf cavity expansion. Furthermore, this transition takes place on the background of declining winter insolation (Berger and Loutre, 1991) which would have acted to further enhance and maintain these changes. This insolation decline has previously been hypothesised as a driver of the Neoglacial increase in coastal sea ice in both Prydz Bay and the Adélie Land regions (Denis *et al.*, 2010), however this monotonic decrease contrasts with the markedly rapid increase in sea ice observed in many records (Fig 4). Our mechanism of ice shelf cavity expansion, reaching a threshold that promoted significant supercooling of continental shelf water masses, reconciles both the rapidity and timing of Neoglacial onset in the middle Holocene.

7. Conclusions and Implications for Antarctic Climate, Sea-Ice and Ice Shelf Behaviour

Our multiproxy record of changing oceanographic conditions in the Adélie Land region indicates a significant meltwater event during the middle Holocene. Comparison of this record with pre-existing studies from around the Antarctic margin indicates this was likely associated with final phases of deglaciation of the Ross Sea embayment. Expansion of the Ross Ice Shelf cavity at this time is proposed to have led to modification of surface water mass formation processes on the continental shelves of the Ross Sea and Adélie Land, and contributed to widespread Antarctic surface water cooling and increased coastal sea ice during the late Holocene Neoglacial. The lack of these coupled ice-ocean processes is apparent in recent Earth system model experiments, in particular the incorporation of evolving ice shelf cavities, with Trace-21k for example, instead simulating a decrease in Antarctic sea-ice extent and thickness after 5 ka (Supplementary Fig. S6). These model outputs are in direct contrast to multiple lines of proxy data in this study and previous work (Steig *et al.*, 1998; Crosta *et al.*, 2008; Denis *et al.*, 2010). Consequently, our results provide insights into the magnitude of this data-model mismatch, as well as a mechanism for rapid sea-ice change and grounding line stabilisation on the background of a warming climate (Liu *et al.*, 2014), both on modern and Holocene time scales. Better representation of the role of evolving ice shelf cavities on oceanic water mass evolution and sea-ice dynamics, which our data indicate acted as a strong negative feedback, will be fundamental to understanding the oceanographic and glaciological implications of future ice shelf loss in the Antarctic.
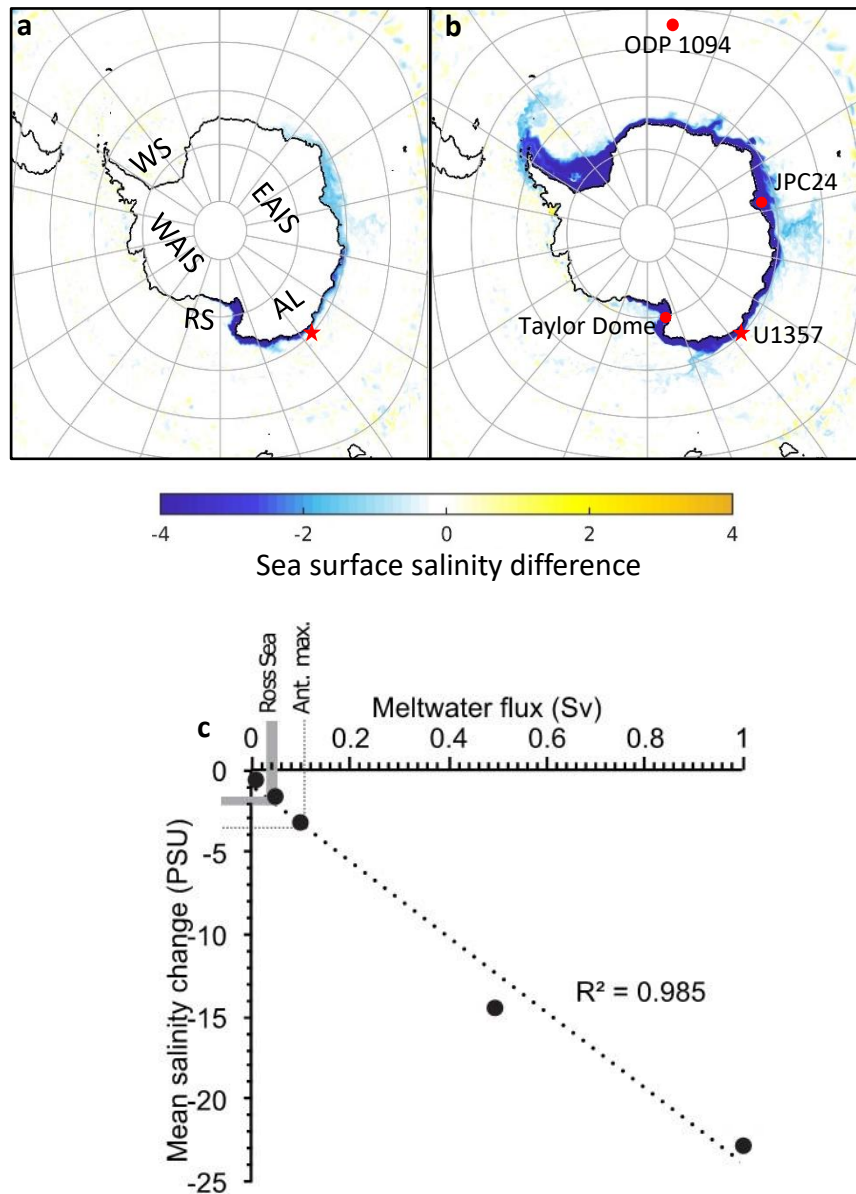
Figures

734
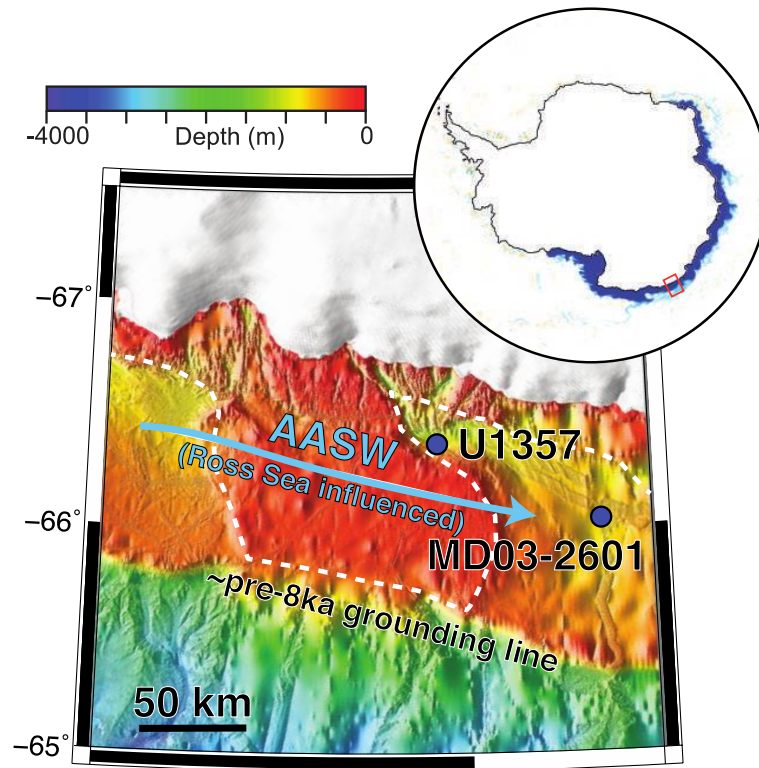
Figure 1: Location of Sites U1357 and MD03-2601 (blue dots). The ice sheet grounding line formed a calving-bay environment (dashed white line) prior to 11.4 ka, but since at least 8.2 ka Antarctic Surface Water flow is largely advected from the Ross Sea (blue line). Inset map: pathway of freshwater (dark blue) after 1 year of 1 Sv meltwater released from along the edge of the Ross Ice Shelf in a model simulation.

Figure 2: MITgcm simulations of meltwater release from along the edge of the Ross Ice Shelf. First two images show sea-surface salinity difference (in practical salinity units) after 3.5 model years resulting from meltwater release volumes of a) 0.1 Sv (2×10^{13} m^3 total ice volume equivalent) and b) 0.5 Sv (1×10^{14} m^3 total ice volume equivalent). Red star indicates position of Site U1357 (this study) and red dots show positions of other core sites mentioned in this study where a Mid-Holocene increase in sea ice and/or cooling is recorded: Taylor Dome (Steig *et al.*, 1998; Baggenstos *et al.*, 2018), JPC24 (Denis *et al.*, 2010) and ODP 1094 (Nielsen *et al.*, 2007). AL = Adélie Land, RS = Ross Sea, WS = Weddell Sea, EAIS = East Antarctic Ice Sheet, WAIS = West Antarctic Ice Sheet. c) Scatter plot of simulated meltwater flux (Sv) against mean salinity difference at U1357 core site. Grey band indicates range of

753 plausible Holocene to deglacial Ross Sea meltwater inputs. Dotted line indicates maximum Antarctic

754 meltwater during the Holocene.

755
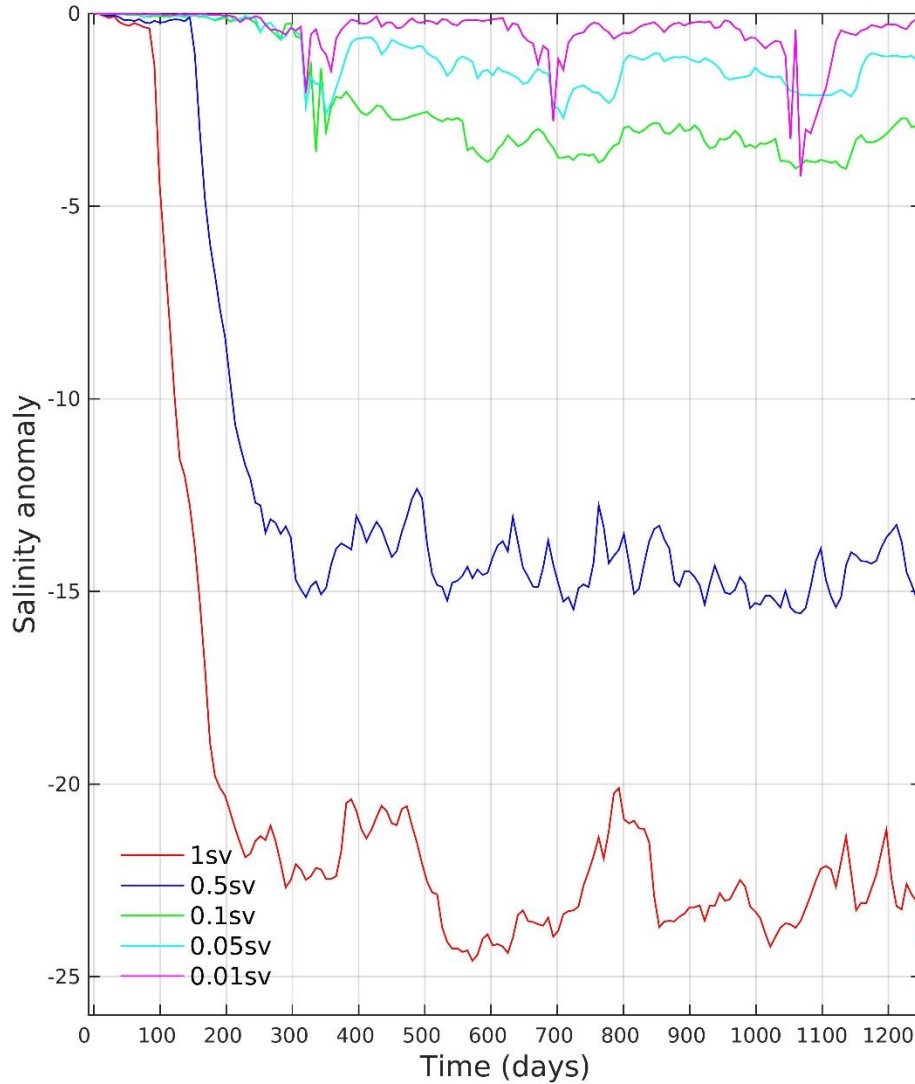
776 **Figure 3** Simulated salinity anomalies over time at Site U1357 for the five meltwater release
777 experiments.
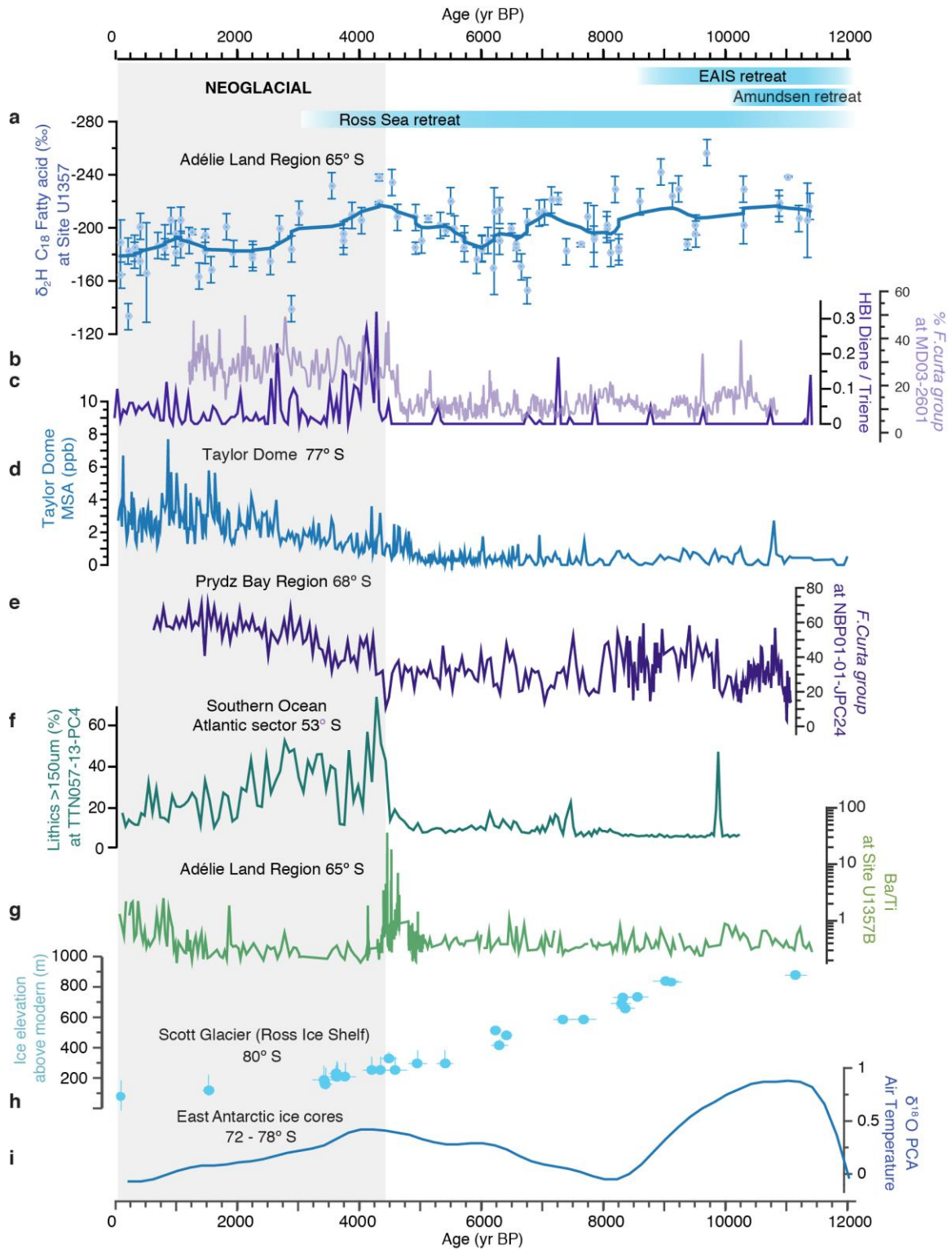
Figure 4: Holocene Adélie Land proxy records from IODP Site U1357 and other circum-Antarctic sites. Glacial retreat chronologies are shown as bars at the top as discussed in the text. a) δ^2H C_{18} fatty

acid at Site U1357 (errors bars based on replicates), with robust locally weighted smoothing (rlowss). b) *Fragilariopsis curta* group (*F. curta* and *F. cylindrus*) relative abundance at MD03-2601, as a proxy of sea-ice conditions (Crosta *et al.*, 2008) c) di-unsaturated HBI ($C_{25:2}$; Diene)/tri-unsaturated HBI isomer ($C_{25:3}$; Triene) ratio at Site U1357 d) Methanesulfonate (MSA) concentrations (ppb) from Taylor Dome ice core e) *F. curta* group relative abundances in core NBP-01-JPC24 f) Coarse lithic (ice-rafted) content at TTN057-13-PC4 (Hodell et al., 2001) g) Ba/Ti (logarithmic scale) at Site U1357 h) [10]Be cosmogenic nuclide ages from Scott Glacier in the SW Ross Ice Shelf region (Spector *et al.*, 2017) i) Temperature signal from principal component analyses of five $\delta^{18}O$ records in five East Antarctic ice cores (Vostok, EPICA Dome C, EPICA Dronning Maud Land, Dome Fuji and Talos Dome) (Masson-Delmotte *et al.*, 2011).

818
819
820
821
822
823
824
825
826
827
828
829
830
831
832
833
834
835
836
837
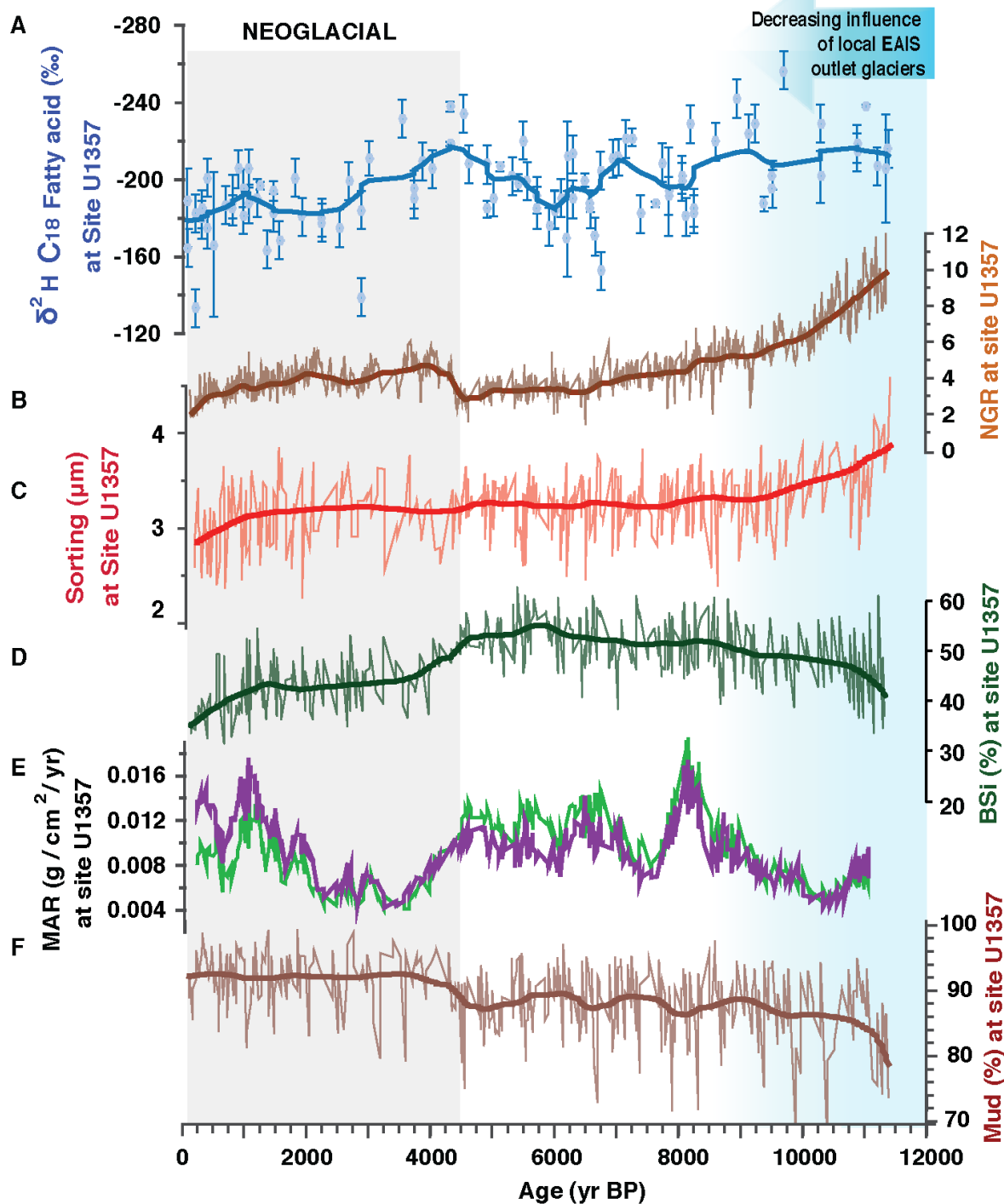838
839
840
841
842
843
844
845
846
847
848
849

Figure 5 Holocene Adélie Land proxy records from IODP Site U1357 a) C$_{18}$ fatty acid δ^2H (errors bars based on replicate analyses), heavy line is a robust locally weighted scatterplot smoothing (rlowss) b) Natural Gamma Radiation, heavy line is a rlowss c) grain sorting (µm) calculated following Folk and Ward (1957), heavy line is a rlowss d) Percentage of biogenic silica (BSi), heavy line is a rlowss; e) Mass accumulation rates of biogenic (green line) and terrigenous (purple line) material f) Percentage of mud, heavy line is a rlowss.
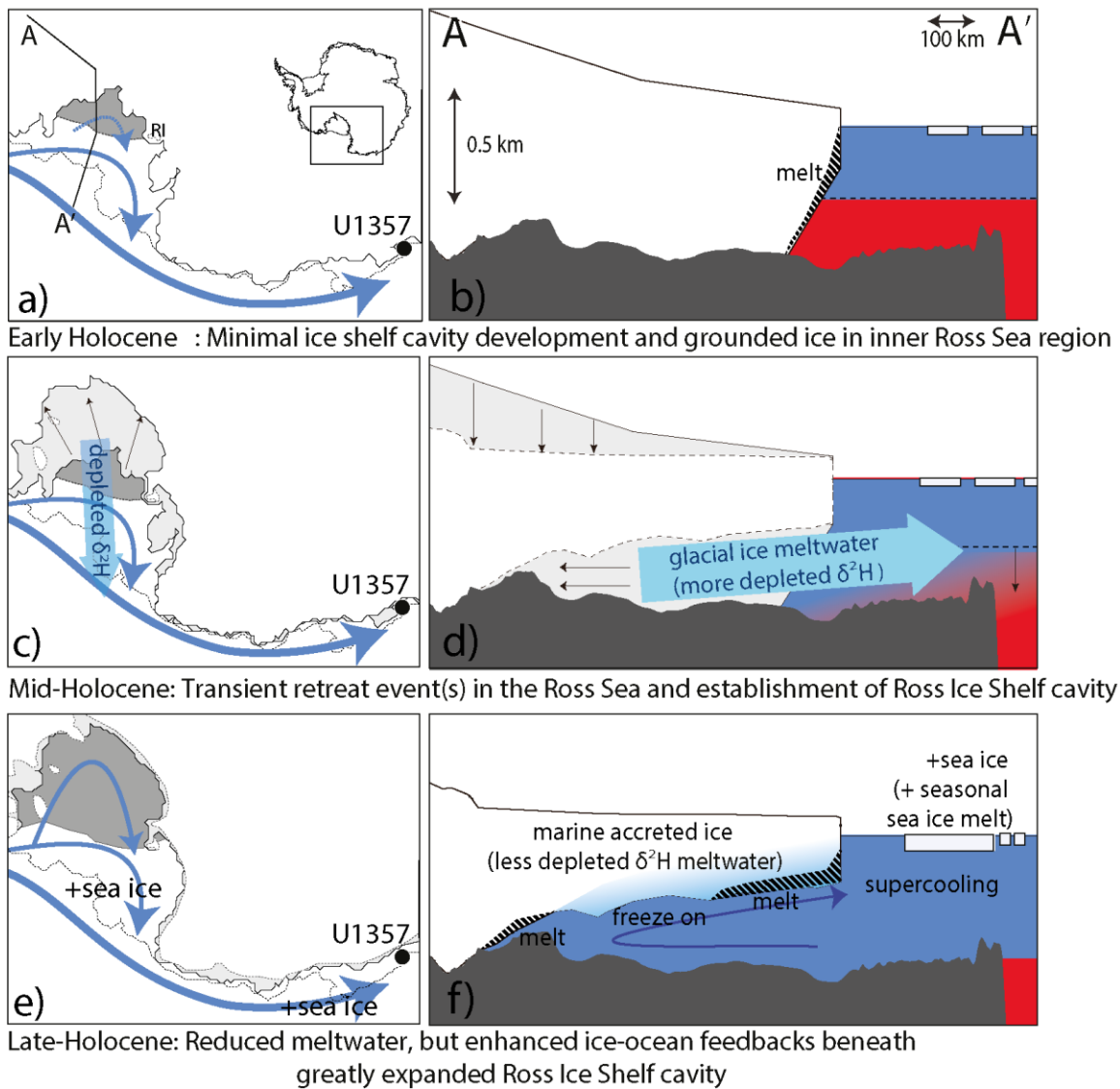
Figure 6: Conceptual model of evolving Holocene glacial and oceanographic conditions in the Ross Sea region. Panels on the left show modelled grounding line positions (McKay *et al.*, 2016), and proposed circulation of surface and sub-ice shelf circulating waters (light blue arrows). Panels on the right show cross sections of the Ross Ice Shelf (RIS) and ice-ocean interactions. Dark blue = cool surface waters, Red = warm subsurface waters. a) The grounding line in Adélie Land is near its modern location, but near Ross Island (RI) in the Ross Sea, and ice shelf cavity (dark grey shading) is reduced in size relative to today (McKay *et al.*, 2016). b) Continental shelf profile A-A' (panel a) shows a Ross Sea grounding line in a mid-continental shelf location in close proximity to the RIS calving line (McKay *et al.*, 2016), with subsurface warming on the continental shelf triggering WAIS deglaciation (Hillenbrand

860 *et al.*, 2017). c) Most grounding line retreat south of RI occurred between 9 and 4.5 ka (light grey

861 shading with black arrows represents area of retreat over this period), proposed to be the consequence of

862 marine ice sheet instability, but the ice shelf calving line remained near its present position (McKay *et*

863 *al.*, 2016; Spector *et al.*, 2017). d) Grounding line retreat and ice shelf thinning released meltwater with

864 negative δ^2H into the surface waters. Increasing ice shelf-oceanic interactions with the development of

865 the ice shelf cavity (dark grey) led to enhanced Antarctic Surface Water formation; f) Minimal

866 grounding line retreat has occurred since 4.5 ka, and the RIS supercools AASW leading to enhanced

867 sea-ice formation despite reduced glacial meltwater flux. Seasonal sea ice meltwater further freshens and

868 cools AASW. Increased production of AASW on the continental shelf leads to isopycnal deepening

869 (dotted line) and limits flow onto the continental shelf slowing further grounding line retreat. However,

870 as the ice shelf is near steady state mass balance and there is a component of marine accreted ice at the

871 base of the ice shelf (Rignot *et al.*, 2013), the strength of the δ^2H signal is reduced relative to periods of

872 mass balance loss.

873

874
875 **References:**
876

877 Adcroft, A. *et al.* (2004) 'Implementation of an Atmosphere–Ocean General Circulation Model on the
878 Expanded Spherical Cube', *Monthly Weather Review*, 132(12), pp. 2845–2863. doi:
879 10.1175/MWR2823.1.

880 Anderson, J. B. *et al.* (2014) 'Ross Sea paleo-ice sheet drainage and deglacial history during and since
881 the LGM', *Quaternary Science Reviews*. Elsevier Ltd, 100, pp. 31–54. doi:
882 10.1016/j.quascirev.2013.08.020.

883 Aoki, S. *et al.* (2013) 'Widespread freshening in the Seasonal Ice Zone near 140°E off the Adélie Land
884 Coast, Antarctica, from 1994 to 2012', *Journal of Geophysical Research: Oceans*, 118(11), pp. 6046–
885 6063. doi: 10.1002/2013JC009009.

886 Arrigo, K. R. and van Dijken, G. L. (2003) 'Phytoplankton dynamics within 37 Antarctic coastal
887 polynya systems', *Journal of Geophysical Research*, 108(C8), p. 3271. doi: 10.1029/2002JC001739.

888 Asper, V. L. and Smith, W. O. (1999) 'Particle fluxes during austral spring and summer in the southern
889 Ross Sea, Antarctica', *Journal of Geophysical Research: Oceans*, 104(C3), pp. 5345–5359. doi:
890 10.1029/1998JC900067.

891 Baggenstos, D. *et al.* (2018) 'A Horizontal Ice Core From Taylor Glacier, Its Implications for Antarctic
892 Climate History, and an Improved Taylor Dome Ice Core Time Scale', *Paleoceanography and*
893 *Paleoclimatology*, 33(7), pp. 778–794. doi: 10.1029/2017PA003297.

894 Beans, C. *et al.* (2008) 'A study of the diatom-dominated microplankton summer assemblages in coastal
895 waters from Terre Adelie to the Mertz Glacier, East Antarctica (139??E-145??E)', *Polar Biology*, 31(9),
896 pp. 1101–1117. doi: 10.1007/s00300-008-0452-x.

897 Belt, S. T. *et al.* (2007) 'A novel chemical fossil of palaeo sea ice: IP25', *Organic Geochemistry*, 38(1),
898 pp. 16–27. doi: 10.1016/j.orggeochem.2006.09.013.

899 Belt, S.T., Smik, L., Brown, T.A., et al. (2016) Source identification and distribution reveals the
900 potential of the geochemical Antarctic sea ice proxy IPSO25. Nature Communications, 7: 12655.
901 doi:10.1038/ncomms12655.

902 Bentley, M. J. *et al.* (2014) 'A community-based geological reconstruction of Antarctic Ice Sheet
903 deglaciation since the Last Glacial Maximum', *Quaternary Science Reviews*, 100, pp. 1–9. doi:
904 10.1016/j.quascirev.2014.06.025.

905 Berger, A. and Loutre, M. F. (1991) 'Insolation values for the climate of the last 10 million years',
906 *Quaternary Science Reviews*, 10(4), pp. 297–317. doi: 10.1016/0277-3791(91)90033-Q.

907 Bindoff, N., Rintoul, S. and Massom, R. (2000) 'Bottom water formation and polynyas in Adelie Land,
908 Antarctica', *Papers and Proceedings of the Royal Society of Tasmania*, 133(3), pp. 51–56. doi:
909 10.26749/rstpp.133.3.51.

910 Brook, E. J. *et al.* (2005) 'Timing of millennial-scale climate change at Siple Dome, West Antarctica,
911 during the last glacial period', *Quaternary Science Reviews*, 24(12–13), pp. 1333–1343. doi:
912 10.1016/j.quascirev.2005.02.002.

913 Budge, S. M. *et al.* (2008) 'Tracing carbon flow in an arctic marine food web using fatty acid-stable
914 isotope analysis', *Oecologia*, 157(1), pp. 117–129. doi: 10.1007/s00442-008-1053-7.

915 Campagne, P. *et al.* (2015) 'Glacial ice and atmospheric forcing on the Mertz Glacier Polynya over the
916 past 250 years', *Nature Communications*, 6. doi: 10.1038/ncomms7642.

917 Condron, A. and Winsor, P. (2012) 'Meltwater routing and the Younger Dryas', *Proceedings of the
918 National Academy of Sciences*, 109(49), pp. 19928–19933. doi: 10.1073/pnas.1207381109.

919 Conway, H., Hall, B.L., Denton, G.H., et al. (1999) Past and Future Grounding-Line Retreat of the West
920 Antarctic Ice Sheet. Science, 286 (5438): 280–283. doi:10.1126/science.286.5438.280.

921 Crosta, X., Denis, D. and Ther, O. (2008) 'Sea ice seasonality during the Holocene, Adelie Land, East
922 Antarctica', *Marine Micropaleontology*, 66(3–4), pp. 222–232. doi: 10.1016/j.marmicro.2007.10.001.

923 Dalsgaard, J. *et al.* (2003) 'Fatty acid trophic markers in the pelagic marine environment', *Advances in
924 Marine Biology*, 46, pp. 225–340. doi: 10.1016/S0065-2881(03)46005-7.

925 DeMaster, D. J. (1981) 'The supply and accumulation of silica in the marine environment', *Geochimica
926 et Cosmochimica Acta*, 45(10), pp. 1715–1732. doi: 10.1016/0016-7037(81)90006-5.

927 Denis, D. *et al.* (2010) 'Sea ice and wind variability during the Holocene in East Antarctica: Insight on

928   middle-high latitude coupling', *Quaternary Science Reviews*, 29(27–28), pp. 3709–3719. doi:
929   10.1016/j.quascirev.2010.08.007.

930   DiTullio, G. R. *et al.* (2000) 'Rapid and early export of Phaeocystis antarctica blooms in the Ross Sea,
931   Antarctica', *Nature*, 404(6778), pp. 595–598. doi: 10.1038/35007061.

932   Domack, E. *et al.* (2006) 'Subglacial morphology and glacial evolution of the Palmer deep outlet
933   system, Antarctic Peninsula', *Geomorphology*, 75(1–2 SPEC. ISS.), pp. 125–142. doi:
934   10.1016/j.geomorph.2004.06.013.

935   Escutia, C. *et al.* (2011) 'Expedition 318 summary', in. doi: 10.2204/iodp.proc.318.101.2011.

936   Etourneau, J. *et al.* (2013) 'Holocene climate variations in the western Antarctic Peninsula: Evidence for
937   sea ice extent predominantly controlled by changes in insolation and ENSO variability', *Climate of the*
938   *Past*, 9(4), pp. 1431–1446. doi: 10.5194/cp-9-1431-2013.

939   Feakins, S. J., Warny, S. and Lee, J.-E. (2012) 'Hydrologic cycling over Antarctica during the middle
940   Miocene warming', *Nature Geoscience*, 5. doi: 10.1038/NGEO1498.

941   Hein, A. S. *et al.* (2016) 'Mid-Holocene pulse of thinning in the Weddell Sea sector of the West
942   Antarctic ice sheet', *Nature Communications*. Nature Publishing Group, 7, p. 12511. doi:
943   10.1038/ncomms12511.

944   Hellmer, H. H. (2004) 'Impact of Antarctic ice shelf basal melting on sea ice and deep ocean properties',
945   *Geophysical Research Letters*, 31(10), pp. 1–4. doi: 10.1029/2004GL019506.

946   Hillenbrand, C. D. *et al.* (2017) 'West Antarctic Ice Sheet retreat driven by Holocene warm water
947   incursions', *Nature*, 547(7661), pp. 43–48. doi: 10.1038/nature22995.
948
949   Hodell, D. A. *et al.* (2001) 'Abrupt Cooling of Antarctic Surface Waters and Sea Ice Expansion in the
950   South Atlantic Sector of the Southern Ocean at 5000 cal yr B.P.', *Quaternary Research*, 56(02), pp.
951   191–198. doi: 10.1006/qres.2001.2252.

952   Holland, D. M., Jacobs, S. S. and Jenkins, A. (2003) 'Modelling the ocean circulation beneath the Ross
953   Ice Shelf', *Antarctic Science*, 15(1), pp. 13–23. doi: 10.1017/S0954102003001019.

954   Huang, Y. *et al.* (1999) 'Glacial-interglacial environmental changes inferred from molecular and
955   compound-specific $\delta 13C$ analyses of sediments from Sacred Lake, Mt. Kenya', *Geochimica et*
956   *Cosmochimica Acta*, 63(9), pp. 1383–1404. doi: 10.1016/S0016-7037(99)00074-5.

957   Hughes, K. *et al.* (2014) 'Extension of an Ice ShelfWater plumemodel beneath sea ice with application
958   inMcMurdo Sound, Antarctica', *Journal of Geophysical Research: Oceans*, 119, pp. 8662–8687. doi:
959   10.1002/2014JC010248.Received.

960   Jacobs, S. S. *et al.* (2004) *Summer Oceanographic Measurements near the Mertz Polynya (140-150E)*
961   *on NB Palmer Cruise 00-08*. doi: 10.15784/601161.

962   Jacobs, S. S., Giulivi, C. F. and Mele, P. A. (2002) 'Freshening of the Ross Sea During the Late 20th

963 Century', *Science*, 297(5580), pp. 386–389. doi: 10.1126/science.1069574.

964 Jensen, S., Renberg, L. and Reutergårdh, L. (1977) 'Residue Analysis of Sediment and Sewage Sludge
965 for Organochlorines in the Presence of Elemental Sulfur', *Analytical Chemistry*, 49(2), pp. 316–318.
966 doi: 10.1021/ac50010a033.

967 Johns, L. *et al.* (1999) 'Identification of a C25highly branched isoprenoid (HBI) diene in Antarctic
968 sediments, Antarctic sea-ice diatoms and cultured diatoms', *Organic Geochemistry*, 30(11), pp. 1471–
969 1475. doi: 10.1016/S0146-6380(99)00112-6.

970 Jones, J. M. *et al.* (2016) 'Assessing recent trends in high-latitude Southern Hemisphere surface
971 climate', *Nature Climate Change*. Nature Publishing Group, 6(10), pp. 917–926. doi:
972 10.1038/nclimate3103.

973 Jourdain, N. C. *et al.* (2017) 'Ocean circulation and sea-ice thinning induced bymelting ice shelves in
974 the Amundsen Sea', *Journal of Geophysical Research: Oceans*, 122(3), pp. 2550–2573. doi:
975 10.1002/2016JC012509.Received.

976 Killops, S. and Killops, V. (2004) *Introduction to Organic Geochemistry*, *Blackwell Publishing Ltd.* doi:
977 10.1002/9781118697214.

978 Kim, J. H. *et al.* (2002) 'Interhemispheric comparison of deglacial sea-surface temperature patterns in
979 Atlantic eastern boundary currents', *Earth and Planetary Science Letters*, 194(3–4), pp. 383–393. doi:
980 10.1016/S0012-821X(01)00545-3.

981 Kim, J. H. *et al.* (2010) 'New indices and calibrations derived from the distribution of crenarchaeal
982 isoprenoid tetraether lipids: Implications for past sea surface temperature reconstructions', *Geochimica*
983 *et Cosmochimica Acta*, 74(16), pp. 4639–4654. doi: 10.1016/j.gca.2010.05.027.

984 Kingslake, J., Scherer, R.P., Albrecht, T., et al. (2018) Extensive retreat and re-advance of the West
985 Antarctic Ice Sheet during the Holocene. Nature, 558 (7710): 430–434. doi:10.1038/s41586-018-0208-x.

986 Kopczynska, E. E. *et al.* (1995) 'Phytoplankton Composition and Cell Carbon Distribution in Prydz
987 Bay, Antarctica - Relation To Organic Particulate Matter and Its Delta-C-13 Values', *Journal of*
988 *Plankton Research*, 17(4), pp. 685–707. doi: 10.1093/plankt/17.4.685.

989 Kusahara, K., Hasumi, H. and Tamura, T. (2010) 'Modeling sea ice production and dense shelf water
990 formation in coastal polynyas around East Antarctica', *Journal of Geophysical Research: Oceans*,
991 115(10), p. C10006. doi: 10.1029/2010JC006133.

992 Leventer, A. *et al.* (2006) 'Marine sediment record from the East Antarctic margin reveals dynamics of
993 ice sheet recession', *GSA Today*, 16(12), pp. 4–10. doi: 10.1130/GSAT01612A.1.

994 Liu, Z. *et al.* (2014) 'The Holocene temperature conundrum', *Proceedings of the National Academy of*
995 *Sciences*, 111(34), pp. E3501--E3505. doi: 10.1073/pnas.1407229111.

997 Lowry, D. P. *et al.* (2019) 'Deglacial grounding-line retreat in the Ross Embayment, Antarctica,
998 controlled by ocean and atmosphere forcing', *Science Advances*. doi: 10.1126/sciadv.aav8754.

Mackintosh, A. N. *et al.* (2014) 'Retreat history of the East Antarctic Ice Sheet since the Last Glacial Maximum', *Quaternary Science Reviews*. Elsevier Ltd, 100, pp. 10–30. doi: 10.1016/j.quascirev.2013.07.024.

Marcott, S. a. *et al.* (2013) 'A Reconstruction of Regional and Global Temperature for the Past 11,300 Years', *Science (New York, N.Y.)*, 339(6124), pp. 1198–1201. doi: 10.1126/science.1228026.

Marshall, J. *et al.* (1997) 'A finite-volume, incompressible Navier Stokes model for studies of the ocean on parallel computers', *Journal of Geophysical Research: Oceans*, 102(C3), pp. 5753–5766. doi: 10.1029/96JC02775.

Marsland, S. J. *et al.* (2004) 'Modeling water mass formation in the Mertz Glacier Polynya and Ad??lie Depression, East Antarctica', *Journal of Geophysical Research: Oceans*, 109(11), p. C11003. doi: 10.1029/2004JC002441.

Massé, G. *et al.* (2011) 'Highly branched isoprenoids as proxies for variable sea ice conditions in the Southern Ocean', *Antarctic Science*, 23(5), pp. 487–498. doi: 10.1017/S0954102011000381.

Massom, R. A. *et al.* (2001) 'Effects of regional fast-ice and iceberg distributions on the behaviour of the Mertz Glacier polynya, East Antarctica', *Annals of Glaciology*, 33, pp. 391–398. doi: 10.3189/172756401781818518.

Massom, R. A. *et al.* (2018) 'Antarctic ice shelf disintegration triggered by sea ice loss and ocean swell', *Nature*. Springer US, (Ii). doi: 10.1038/s41586-018-0212-1.

Masson-Delmotte, V. *et al.* (2011) 'A comparison of the present and last interglacial periods in six Antarctic ice cores', *Climate of the Past*, 7(2), pp. 397–423. doi: 10.5194/cp-7-397-2011.

Matsuda, H. (1978) 'Early diagenesis of fatty acids in lacustrine sediments-III. Changes in fatty acid composition in the sediments from a brackish water lake', *Geochimica et Cosmochimica Acta*, 42, pp. 1027–1034.

Mayer, L. M. (1993) 'Organic Matter at the Sediment-Water Interface', in *Organic Geochemistry: principles and applications*, pp. 171–184. doi: 10.1007/978-1-4615-2890-6_7.

McCartney, M. S. and Donohue, K. A. (2007) 'A deep cyclonic gyre in the Australian-Antarctic Basin', *Progress in Oceanography*, 75(4), pp. 675–750. doi: 10.1016/j.pocean.2007.02.008.

McCave, I. N. and Hall, I. R. (2006) 'Size sorting in marine muds: Processes, pitfalls, and prospects for paleoflow-speed proxies', *Geochemistry, Geophysics, Geosystems*, 7(10). doi: 10.1029/2006GC001284.

McCave, I. N., Manighetti, B. and Robinson, S. G. (1995) 'Sortable silt and fine sediment size/composition slicing: Parameters for palaeocurrent speed and palaeoceanography', *Paleoceanography*, 10(3), pp. 593–610. doi: 10.1029/94PA03039.

McKay, R. *et al.* (2016) 'Antarctic marine ice-sheet retreat in the Ross Sea during the early Holocene', *Geology*, 44(1), pp. 7–10. doi: 10.1130/G37315.1.

Meyers, P. A. and Ishiwatari, R. (1993) 'Lacustrine organic geochemistry-an overview of indicators of organic matter sources and diagenesis in lake sediments', *Organic Geochemistry*, 20(7), pp. 867–900. doi: 10.1016/0146-6380(93)90100-P.

Mezgec, K. *et al.* (2017) 'Holocene sea ice variability driven by wind and polynya efficiency in the Ross Sea', *Nature Communications*. Springer US, 8(1). doi: 10.1038/s41467-017-01455-x.

Nielsen, S. H. H. *et al.* (2007) 'Origin and significance of ice-rafted detritus in the Atlantic sector of the Southern Ocean', *Geochemistry, Geophysics, Geosystems*, 8(12), p. n/a-n/a. doi: 10.1029/2007GC001618.

Pagani, M. *et al.* (2006) 'Arctic hydrology during global warming at the Palaeocene/Eocene thermal maximum', *Nature*, 442(7103), pp. 671–675. doi: 10.1038/nature05043.

Paolo, F. S., Fricker, H. A. and Padman, L. (2015) 'Volume loss from Antarctic ice shelves is accelerating', *Science*, 348(6232), pp. 327–331. doi: 10.1126/science.aaa0940.

Peña-Molino, B., McCartney, M. S. and Rintoul, S. R. (2016) 'Direct observations of the Antarctic Slope Current transport at 113°E', *Journal of Geophysical Research: Oceans*. doi: 10.1002/2015JC011594.

Peters, K. E. and Moldowan, J. M. (1993) 'The biomarker guide: interpreting molecular fossils in petroleum and ancient sediments', *The biomarker guide: interpreting molecular fossils in petroleum and ancient sediments*. doi: 10.5860/choice.30-2690.

Pollard, D. and Deconto, R. M. (2016) 'Contribution of Antarctica to past and future sea-level rise', *Nature*, 531(7596), pp. 591–597. doi: 10.1038/nature17145.

Potter, J. R. and Paren, J. G. (1985) 'Interaction between ice shelf and ocean in George VI Sound, Antarctica', in *Oceanology of the Antarctic Continental Shelf (ed S. S. Jacobs)*, pp. 35–58. doi: 10.1029/AR043p0035.

Rhodes, R. H. *et al.* (2012) 'Little Ice Age climate and oceanic conditions of the Ross Sea, Antarctica from a coastal ice core record', *Climate of the Past*, pp. 1223–1238. doi: 10.5194/cp-8-1223-2012.

Riaux-Gobin, C. *et al.* (2011) 'Spring phytoplankton onset after the ice break-up and sea-ice signature (Adelie Land, East Antarctica)', *Polar Research*, 30(SUPPL.1). doi: 10.3402/polar.v30i0.5910.

Riaux-Gobin, C. *et al.* (2013) 'Environmental conditions, particle flux and sympagic microalgal succession in spring before the sea-ice break-up in Adélie Land, East Antarctica', *Polar Research*, 32, pp. 0–25. doi: 10.3402/polar.v32i0.19675.

Rignot, E. *et al.* (2013) 'Ice Shelf Melting Around Antarctica', *Science*, 1(June), pp. 1–15. doi: 10.1126/science.1235798.

Riis, V. and Babel, W. (1999) 'Removal of sulfur interfering in the analysis of organochlorines by GC-ECD', *Analyst*, 124(12), pp. 1771–1773. doi: 10.1039/a907504f.

Robinson, N. J. *et al.* (2014) 'Evolution of a supercooled Ice Shelf Water plume with an actively growing subice platelet matrix', *Journal of Geophysical Research : Oceans*, pp. 3425–3446. doi: 10.1002/2013JC009399.Received.

Sachse, D. *et al.* (2012) 'Molecular Paleohydrology: Interpreting the Hydrogen-Isotopic Composition of Lipid Biomarkers from Photosynthesizing Organisms', *Annual Review of Earth and Planetary Sciences*, 40(1), pp. 221–249. doi: 10.1146/annurev-earth-042711-105535.

Schmidt, G. A., Bigg, G. R. and Rohling, E. J. (1999) *Global Seawater Oxygen-18 Database - v1.22*. Available at: https://data.giss.nasa.gov/o18data/.

Schoemann, V. *et al.* (2005) 'Phaeocystis blooms in the global ocean and their controlling mechanisms: A review', *Journal of Sea Research*, pp. 43–66. doi: 10.1016/j.seares.2004.01.008.

Schouten, S. *et al.* (2006) 'The effect of temperature, salinity and growth rate on the stable hydrogen isotopic composition of long chain alkenones produced by *Emiliania huxleyi* and *Gephyrocapsa oceanica*', *Biogeosciences*, 3(1), pp. 113–119. doi: 10.5194/bg-3-113-2006.

Sessions, A. L. *et al.* (1999) 'Fractionation of hydrogen isotopes in lipid biosynthesis, Org', *Organic Geochemistry*, 30, pp. 1193–1200. doi: 10.1016/S0146-6380(99)00094-7.

Sessions, A. L. *et al.* (2004) 'Isotopic exchange of carbon-bound hydrogen over geologic timescales', *Geochimica et Cosmochimica Acta*, 68(7), pp. 1545–1559. doi: 10.1016/j.gca.2003.06.004.

Shackleton, N. J. and Kennett, J. P. (1975) 'Paleotemperature history of the Cenozoic and the initiation of Antarctic glaciation; Oxygen and carbon isotope analyses in DSDP sites 277, 279 and 281', *Initial Reports of the Deep Sea Drilling Project*, 29, pp. 743–755. doi: 10.2973/dsdp.proc.37.1977.

Smethie, W. M. and Jacobs, S. S. (2005) 'Circulation and melting under the Ross Ice Shelf: Estimates from evolving CFC, salinity and temperature fields in the Ross Sea', *Deep-Sea Research Part I: Oceanographic Research Papers*, 52(6), pp. 959–978. doi: 10.1016/j.dsr.2004.11.016.

Smik, L., Belt, S.T., Lieser, J.L., et al. (2016) Distributions of highly branched isoprenoid alkenes and other algal lipids in surface waters from East Antarctica: Further insights for biomarker-based paleo sea-ice reconstruction. Organic Geochemistry, 95: 71–80. doi:10.1016/j.orggeochem.2016.02.011.

Smith Jr., W. O. *et al.* (2012) 'the Ross Sea in a Sea of Change', *Oceanography*, 25(3, SI), pp. 90–103.

Solomina, O. N. *et al.* (2015) 'Holocene glacier fluctuations', *Quaternary Science Reviews*, pp. 9–34. doi: 10.1016/j.quascirev.2014.11.018.

Spector, P. *et al.* (2017) 'Rapid early-Holocene deglaciation in the Ross Sea, Antarctica', *Geophysical Research Letters*, 44(15), pp. 7817–7825. doi: 10.1002/2017GL074216.

Steig, E. J. *et al.* (1998) 'Changes in climate, ocean and ice sheet conditions in the Ross Embayment at 6 ka', *Annals of Glaciology*, 27, pp. 305–310. doi: 10.3198/1998AoG27-1-305-310.

Strickland, J. D. and Parsons, T. R. (1970) 'J. D. H. Strickland and T. R. Parsons: A Practical Handbook

1103 of Seawater Analysis. Ottawa: Fisheries Research Board of Canada, Bulletin 167, 1968. 293 pp. $ 7.50',
1104 in *Internationale Revue der gesamten Hydrobiologie und Hydrographie*, pp. 167–167. doi:
1105 10.1002/iroh.19700550118.

1106 Tang, K. W. *et al.* (2008) 'Colony size of Phaeocystis antarctica (Prymnesiophyceae) as influenced by
1107 zooplankton grazers', *Journal of Phycology*, 44(6), pp. 1372–1378. doi: 10.1111/j.1529-
1108 8817.2008.00595.x.

1109 Todd, C., Stone, J., Conway, H., et al. (2010) Late Quaternary evolution of Reedy Glacier, Antarctica.
1110 Quaternary Science Reviews, 29 (11–12): 1328–1341. doi:10.1016/j.quascirev.2010.02.001.

1111 Turner, J. *et al.* (2016) 'Antarctic sea ice increase consistent with intrinsic variability of the Amundsen
1112 sea low', *Climate Dynamics*. Springer Berlin Heidelberg, 46(7–8), pp. 2391–2402. doi: 10.1007/s00382-
1113 015-2708-9.

1114 Wong, W. W. and Sackett, W. M. (1978) 'Fractionation of stable carbon isotopes by marine
1115 phytoplankton', *Geochimica et Cosmochimica Acta*, 42(12), pp. 1809–1815. doi: 10.1016/0016-
1116 7037(78)90236-3.

1117 Zhang, J. and Hibler, W. D. (1997) 'On an efficient numerical method for modeling sea ice dynamics',
1118 *Journal of Geophysical Research*, 102(C4), p. 8691. doi: 10.1029/96JC03744.

1119 Zhang, Z., Sachs, J. P. and Marchetti, A. (2009) 'Hydrogen isotope fractionation in freshwater and
1120 marine algae: II. Temperature and nitrogen limited growth rate effects', *Organic Geochemistry*, 40(3),
1121 pp. 428–439. doi: 10.1016/j.orggeochem.2008.11.002.
1122
1123

1135
1136 **Author contributions:** K.E.A., J.B and R.M. wrote the paper. J.B. and O.S. carried out the fatty acid
1137 isotope analysis, A.A. and R.M. conducted the grain size analyses, J.E. and G.M. generated the HBI
1138 data, F.J.J.E measured X-ray fluorescence scanning and electron microscopy, and C.R conducted the
1139 opal measurements. R.D., R.M., X.C. and G.M. developed the age model. A.C ran the model
1140 simulations. D.P.L and E.G analysed the Trace-21k experiment data. R.D. was lead proponent on the

1141 U1357 drilling proposal. All authors contributed to the interpretations of data and finalization of the
1142 manuscript.
1143
1144 **Competing interests:** The authors have no competing interests.
1145
1146 **Data availability:** There is no restriction on data availability. Upon manuscript acceptance, all
1147 previously unpublished data will be added to the Supplementary Materials and made freely available at
1148 the NOAA NCDC data-base: https://www.ncdc.noaa.gov/data-access/paleoclimatology-data/datasets.
1149
1150
1151